On the statistics of coherent vortices in incoherent environments

Tobias Bölle

Physica A 612 (2023) 128473

Contents lists available at ScienceDirect

Physica A

journal homepage: www.elsevier.com/locate/physa

On the statistics of coherent vortices in incoherent environments

Tobias Bölle *

Deutsches Zentrum für Luft- und Raumfahrt, Institut für Physik der Atmosphäre, Oberpfaffenhofen, Germany
DAAA, ONERA-The French Aerospace Lab, Université Paris Saclay, 8 Rue des Vertugadins, 92190, Meudon, France

ARTICLE INFO

Article history:
Received 29 July 2022
Received in revised form 12 December 2022
Available online 14 January 2023

Keywords:
Vortex meandering
Brownian motion
Gauss–Markov process

ABSTRACT

Coherent vortices are important building blocks of complex flows on all scales, governing dynamics in various applications from geophysics over engineering to the coherent-structures' paradigm of turbulence. As a commonly studied prototype of this configuration, we consider a large-scale, line vortex evolving in a background flow of small-scale, incoherent turbulence, which, nevertheless, naturally occurs in trailing vortices and tornadoes. The main unsteadiness of the large-scale vortex in this configuration is called meandering. Despite a common observation in experiments since the 1970s and a multitude of studies, its origin and physical mechanism remain puzzling as of this writing. Nevertheless, we do have considerable experimental evidence that, in the range of typically assumed parameters, vortex meandering shares four universal characteristics; namely, (*i*) fluctuations of the vortex-centre position obey a Gaussian distribution with (*ii*) monotonously growing standard deviation downstream. Besides, (*iii*) the fluctuation kinetic energy and enstrophy increase downstream, whereas the main contribution comes from a dipolar vorticity fluctuation pattern confined to the vortex core. This corresponds to the (*iv*) typical spectral signature of power spectra spanning all resolved scales, whereas the variance level increases monotonously towards the low frequencies. We present the first theoretical model to explain all four experimental cornerstones of vortex meandering in one theory. Starting from the definition of the vortex centre, we first show that the meandering motion is linearly proportional to the leading expansion coefficients of a Karhunen–Loève decomposition of the vorticity field. This has been conjectured before but has never been shown. The configuration strongly suggests scale separation between the response times of the vortex and the surrounding turbulence. On this assumption, we derive a Langevin equation for the slow, large scales driven by the fast, small scales, represented as a stochastic forcing. The particular phenomenon of vortex meandering therewith is found to belong to the large class of Gauss–Markov processes. That is, vortex meandering is an (abstract) Brownian motion. From this understanding, we infer immediately that the Gaussian statistics are a consequence of the central limit theorem and that the growing standard deviation follows from a competition between external forcing and intrinsic resistance. In the equilibrium limit, we derive the spectral signature of the large scales as a power law of the frequency, response time and forcing variance. Eventually, comparing our theoretical model with an experimental database gathered at the ONERA, we find good overall agreement.

* Correspondence to: Deutsches Zentrum für Luft- und Raumfahrt, Institut für Physik der Atmosphäre, Oberpfaffenhofen, Germany.
E-mail address: tobias.boelle@dlr.de.

https://doi.org/10.1016/j.physa.2023.128473

1. Introduction

Einstein and Smoluchowski's theoretical work on Brownian motion [1,2], experimentally confirmed by [3], laid the foundation for the general acceptance of an atomistic reality of matter. According to this understanding, the homogeneity of matter is apparent, while it is actually a discontinuous composition of recurrent, elementary building blocks [3]. We see a conceptual parallel in the coherent-structures' paradigm of turbulence. While formally described by continuous field equations, there is the common expectation that turbulence can in fact be understood as an interplay between some recurrent, elementary building blocks, called coherent structures [4,5].

The dynamics of an isolated slender line vortex embedded in incoherent background turbulence of much shorter and smaller scale is a common abstraction for studying coherent structures [6–8], trailing vortices in the intermediate wake (defined as the downstream range where the vortex is fully formed, while the mutual influence of the vortex pair is yet negligible) [9,10] and comparable configurations [11,12]. As a common feature, this dynamics is characterised by an irregular, erratic motion of the coherent vortex spanning all resolved scales with the variance levels increasing towards the slow frequencies. The bulk contribution to the variance stems from a slow, lateral undulation of the vortex as a whole called meandering. This motion constitutes the main manifestation of vortex unsteadiness and can be seen as the prototype of unsteady vortex dynamics in the intermediate wake behind lifting surfaces [13]. Nevertheless, we expect the governing dynamics of (vortex) meandering to hold beyond this particular configuration; namely, whenever the actual flow problem can faithfully be abstracted as being the slow response of a persistent large-scale coherent structure to fast small-scale forcing.

With this generalisation in mind, for definiteness, we consider the dynamics of an isolated trailing vortex evolving in the intermediate wake as an experimental means to realise the vortex–turbulence interaction. Vortex meandering is observed in experimental realisations of this configuration since the 1970s [14,15], however, the reason for its occurrence remains puzzling in essential aspects as of this writing [16–18]. While early studies attributed vortex meandering mainly to the disturbing effect of the unavoidable residual turbulence in wind-tunnel experiments [14,15,19], the last twenty years showed manly attempts to explain its origin through (linear) deterministic vortex dynamics, namely some sort of an intrinsic amplification mechanism [13,18,20–22]. However, to the best of our knowledge, none of these approaches was able to explain vortex meandering in its essential features. It seems that one major problem that hampered an earlier explanation is that, despite the phenomenon being intuitively tangible, vortex meandering lacks a definition. Rather than attempting a definition, we maintain that vortex meandering is associated with a small number of universal characteristics of which we possess considerable experimental evidence. We then develop a theoretical model that explains these experimental key features.

1.1. The universal meandering characteristics

In order to elucidate these generic features, let us first recall that meandering designates the lateral displacement of the vortex as a whole. We emphasise the integral character of this notion, bearing a conceptual similarity to the motion of a macroscopic particle. It follows at once the equivalence of meandering to the motion of any fixed point in the vortex. It is customary to consider the space–time series of the vortex-centre position $\boldsymbol{X}(n,t) \in \mathbb{R}^2$ (as defined in Section 3), where n and t, respectively, denote the measurement and evolution time (proportional to the downstream coordinate z) as defined in Section 2. In order to account for the strong variability, we assume $(n,t) \mapsto \boldsymbol{X}(n,t)$ to be a centred random process. We have unanimous experimental evidence that the vortex centre obeys the Gaussian distribution

$$X_i(t) \sim \mathcal{N}(0, \sigma_i^2(t)) \quad (i = 1, 2) \tag{1}$$

over all experimentally probed measurement ranges so far. The standard deviation $\sigma_i(t) := \sqrt{\overline{X_i^2}}(t)$ $(i = 1, 2)$ is called meandering amplitude. Gaussian distribution was in fact already inferred by [15] and was later assumed in the studies of [19]. Experimental validation of (1) are due to [16,23]. For the standard deviation, all experiments indicate monotonic, algebraic growth [16,17,19,24]. In analogy to Taylor's law for the diffusion of a particle in homogeneous turbulence [24,25] proposed the empirical law

$$\frac{\sqrt{\overline{X_i^2}}(t)}{\ell_1} \sim \frac{u}{U_\infty}\sqrt{\frac{zU_\infty}{\Gamma}}, \quad t = zU_\infty^{-1} \quad (i = 1, 2) \tag{2}$$

for the meandering amplitude (normalised on the initial vortex-core radius ℓ_1). Herein, uU_∞^{-1} and Γ denote the turbulence intensity of the (wind-tunnel) experiment and the vortex circulation, respectively. A comparison of (2) with data extracted from the literature is displayed in Fig. 1, showing good agreement for very different settings. In fact, already [15] suggested to model meandering as a diffusion dynamics, the amplitude of which evolves as $\sigma_i(t) \sim \sqrt{\nu_e t}$ for some effective viscosity ν_e. It is easy to see that both models can be related by a simple mixing-length argument. For completeness, we mention that [19] assumed a similar law as part of their correction algorithm.

The growth of the meandering amplitude is parallelled by the amplification of fluctuation kinetic energy and enstrophy in the vortex core [22,23,26]. Karhunen–Loève (KL) decomposition reveals that the bulk contribution to the variance stems from a pair of orthogonally rotated dipole patterns in the fluctuation vorticity confined to the vortex core [22,23,27–29].

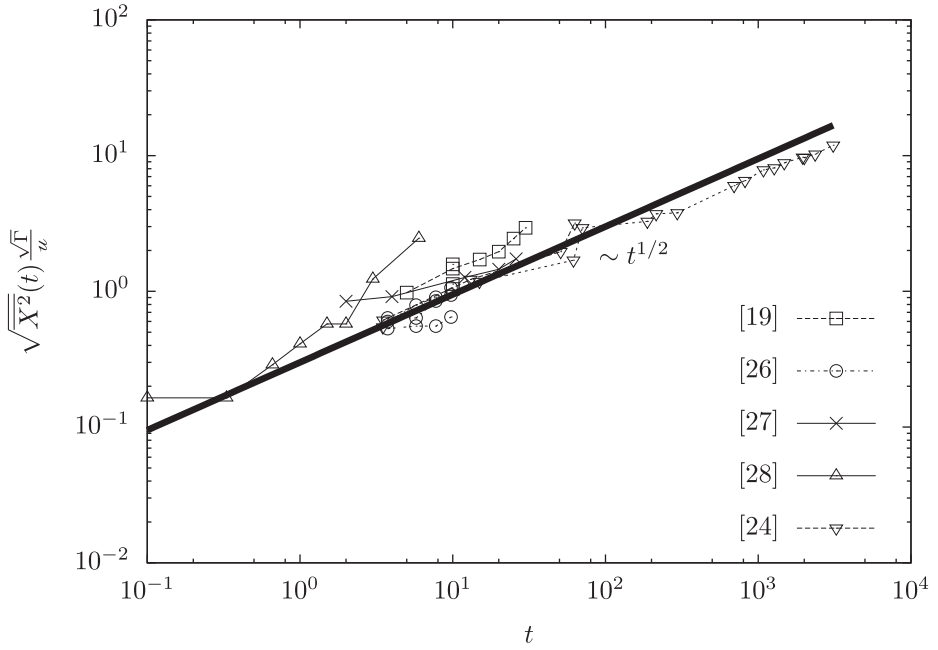

Fig. 1. Meandering-amplitude growth according to (2) compared with data extracted from the literature. The parameters used in the normalisation are listed in Table A.2 of Appendix.

As a last fundamental characteristic, vortex meandering is always associated with a broadband spectral signature spanning all resolved scales, whereas the variance levels increase towards the low frequencies [13,19,30,31]. In particular, the meandering frequencies are much lower than those associated with the turbulent motion [23]. Some controversy was centred around the interpretation of these power spectra. While early studies took the broadband signature as evidence for excitation by the free-stream turbulence [14], variance amplification at low frequencies and the peaky structure of premultiplied power spectra led to the expectation that one meandering frequency could be identified [27,28,31]. Within the scope of the model introduced in the following, we can decide in this question.

The paper is organised as follows. In Section 2 we introduce the canonical experiment leading to vortex meandering and suggest a stochastic interpretation. On this basis, we start the derivation of our meandering model with the experimentally admissible definition of the vortex-centre position X_i in Section 3 and show that in a fixed measurement plane $X_i(t) \sim c_i(t)$ $(i = 1, 2)$, when $c_i(t)$ are the leading KL expansion coefficients. Assuming scale separation between the forcing and response scales, we show that the c_i are governed by a Langevin equation in Section 4, the solutions of which are different Gauss–Markov processes depending on the integration time. In the equilibrium limit (in the measurement time), we derive the response power spectrum and the corresponding correlation function. We compare this vortex-meandering model with an experimental database in Section 5. Finally, we discuss some immediate features and corollaries of the developed theory before concluding in Section 6.

2. The canonical experiment and the conceptual model

We understand vortex meandering as a fundamentally stochastic phenomenon, the framework of which we set out in this section. First, we elaborate an interpretation of the canonical (wind-tunnel) experiment in terms of a random experiment. We then discuss our phenomenological model in which we understand meandering to be a manifestation of a Brownian motion of the vortex as a consequence of a random excitation by the free-stream turbulence.

2.1. The canonical experiment

To the best of our knowledge, vortex meandering has been observed for all experimental settings, facilities and with all measurement techniques, provided the study region extends somewhere between completion of roll up and the onset of secondary dynamics (e.g. mutual instabilities, breakdown, etc..). Therefore, without loss of generality, we can restrict to the canonical experiment of the flow past a rectangular lifting surface of chord length c being mounted at rest in a wind tunnel. The wind tunnel is running at the mean inflow velocity U_∞, set such that $R_c := cU_\infty/\nu \gg 1$. Perturbations contained in the free stream (e.g. originating from the installation) are globally characterised by the turbulence intensity $uU_\infty^{-1} \ll 1$, assumed to be small.

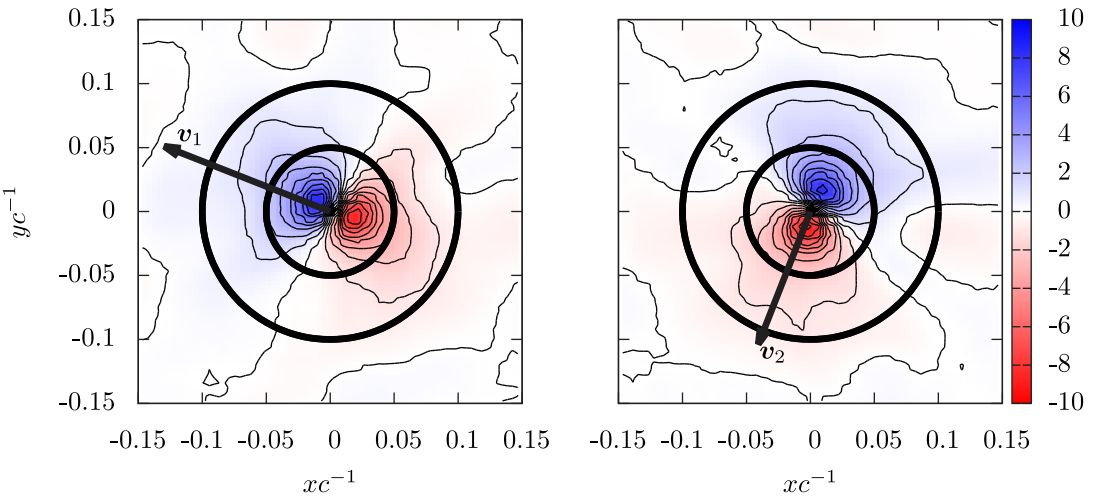

Fig. 2. Leading KL modes of the fluctuation vorticity (arbitrary units) in the last measurement plane of the experiment (cf. Section 5), aligned with the eigenvectors $\boldsymbol{v}_1, \boldsymbol{v}_2$ of the vortex-centre covariance matrix. The inner and outer circle delimit the vortex core (radius ℓ_1) and support (radius ℓ), respectively.

We take the outermost vertex of the trailing edge as the origin of the coordinate system, choosing $x_3 = z$ to point in the direction of the mean inflow velocity U_∞. We call the transverse planes for which $x_3 = z$ is everywhere normal a measurement plane $M \subset \mathbb{R}^2$ and use two sets of orthogonal coordinates as a span; x, y denote the coordinates pointing inwards and vertically upwards, respectively, while it is further convenient to identify x_1, x_2 with the coordinates along the principal axes of the meandering vortex-centre process (see Section 3). Evidently, x, y and x_1, x_2 are two sets of orthogonal, mutually rotated coordinates and we write $\boldsymbol{x} \in M$ for both sets if the distinction is obvious or inessential.

Although trailing vortices inevitably form as a counter-rotating pair of equal strength, the mutual influence in the measurement range of interest only amounts to the induction of a mean motion. We can therefore restrict to an isolated vortex subject to down- and inward drift [19]. Vortex meandering may be understood as the leading-order error that the vortex be found on this mean-drift trajectory.

As an experimentally accessible characteristic length scale, we defined the vortex-core radius $\ell_1 := \arg\max_r \bar{u}_\theta(r)$, where r is the radial coordinate from the vortex centre and $\bar{u}_\theta$ the mean azimuthal velocity in the meandering frame of reference. We expect the characteristic (coherent-vortex) meandering length scale ℓ to be somewhat larger, $\sim 2 \ldots 3 \times \ell_1$, cf. Fig. 2 In the meandering frame, the vortex diffuses at an almost viscous rate so that ℓ is approximately constant over the dynamical scales of interest. We thus assume a dichotomy of the whole fluid domain into the vortex (core), being associated with the fluid contained in the cylinder of radius ℓ around the vortex centre, and its set complement called free stream.

Experiments usually provide us with Eulerian fields of the kind $f(n, x, y, z)$, where $n \in [0, N-1]$ denotes the measurement time (in practice a discrete sample) and $\boldsymbol{x} = (x, y)$ are the coordinates in the measurement plane M at some fixed z downstream of the wing. We suppose that the experiment has been started at a time n_0 and let $n_0 \to -\infty$ in order that the initial condition has been forgotten and the dynamics has settled to a stationary state where the vortex is in equilibrium with the surrounding perturbations. By the ergodic hypothesis, we may think of $z \mapsto (\boldsymbol{x} \mapsto f^{(n)}(\boldsymbol{x}, z))$ as the nth realisation of the vector-valued random process in z (with values in an appropriate function space F over M) [32]. This suggests that it is actually the downstream coordinate that should be interpreted as the evolution time t. We therefore assume a Galilean transformation into the reference frame moving at the velocity $U_\infty = \text{const}$ to equate downstream and temporal evolution, noting $t = zU_\infty^{-1}$. Validity of this association is supported by the experimental finding that typically $\sqrt{\overline{u_z'^2}}U_\infty^{-1} \ll 1$ [26,30,33,34] and the streamwise correlation analysis of [13]. We are thus to consider random processes of the form $t \mapsto f^{(n)}(t) \in F$, where n runs over the various realisations of the experiment in one plane (i.e. for fixed evolution time t) and t corresponds to measurements being taken in planes which are located gradually farther downstream.

2.2. Conceptual model: vortex meandering as a form of Brownian motion

All previous attempts to explain vortex meandering broadly belong to either one of two families which we may call extrinsic and intrinsic dynamics. Regarding the former, we notice that (1)–(2) are the typical signature of a diffusion dynamics. In its simplest form, this would be consistent with the early held idea that meandering is the "beating about" of the vortex by the surrounding free-stream turbulence [14,15,19]. We emphasise the passive role played by the vortex in this picture, while it is typically attributed primary importance for the governance of fluid flows.

In this vein and on account of the typically weak turbulence levels in experiments, meandering was argued to be due to an intrinsic vortex dynamics. Moreover, structural resemblance of the leading vortex-response mode with the least damped, *stable* eigenfunctions of the linearised Navier–Stokes operator of rotational symmetry $|m| = 1$ with m the azimuthal wave number [35,36], was considered as indicating an instability as the origin of vortex meandering [17,18,22]. Albeit, [16] concluded that vortex meandering is essentially stochastic and core fluctuations of helical symmetry merely a secondary effect of the self induction exerted by the meandering vortex on itself. In any event, experimental vortices tend to be highly stable and to the best of our knowledge a definite relation between meandering and a linear instability has never been established. In fact, in an externally driven dynamics, we must search for the *stabilising* features rather than for an instability [37,38].

Indeed, a closer look into the typical scaling behaviour of vortex meandering suggests an interplay between external driving and intrinsic stabilising mechanisms. To this end, we recall the unanimous experimental evidence that vortex meandering is amplified as the turbulence intensity u in the experiment is increased, while meandering is weaker the stronger the vortex (commonly quantified in terms of the circulation Γ) is. This is indicative of vortex meandering in fact being the result of two competing mechanisms: (*i*) an external forcing that drives the vortex out of equilibrium and (*ii*) the intrinsic resistance of the vortex to such deflections. We find this competition expressed in (2), which is directly proportional to u, while it depends reciprocally on Γ. We also note that this proportionality with respect to the forcing strength indicates a linear dynamics.

Concerns about the validity of (2) have been raised by [16] namely for the fact that u appears as a constant (due to Taylor's assumption of homogeneous turbulence) and that meandering must vanish in the absence of external forcing by the free stream $u \to 0^+$. We address these points in the following, however, emphasise an, in our eyes, still more serious issue; namely, a random process for which the standard deviation increases according to (2) for all t is non-homogeneous, meaning that the vortex position gradually diverges without bound. Our results show that this behaviour only applies for intermediate times (in a definite sense), while the amplitude depends on the initial condition for $t \to 0^+$ and approaches an asymptotic equilibrium state in the hypothetical situation that the experimental conditions can be maintained stochastically unchanged.

We find in vortex meandering the paradigm of low-frequency, small-amplitude variability of a comparably large-scale structure in an otherwise rapidly fluctuating environment. This slow response of a large-scale system to fast excitation is reminiscent of a Brownian motion. It is well known that the theory of Brownian motion extends far beyond the original application of a particle suspended in a fluid [1,39]. In fact, the omnipresence of Brownian motion for all macroscopic systems subject to agitation by an environment of relatively small-scale objects independently of the experimental configuration has been identified as one of the main characteristics [2]. Notable applications include finance, fluid–particle dispersion [25], cosmology [40], quantum mechanics [41], climate modelling [37] as wall as biology, chemistry and sociology [42,43]. Meandering therefore does not appear as the apparently highly special problem but integrates into a large family of problems. [44] resumes, "nonequilibrium systems, when they deviate only slightly from equilibrium, …are well described on the macroscopic level by a Gauss–Markov process". To the best of our knowledge, the idea to understand vortex meandering as a manifestation of an abstract Brownian motion was proposed only recently by [45].

Our qualitative model is as follows. We imagine one large-scale vortex evolving in a bath of very many small-scale eddies distributed at random (modelling the free-stream turbulence). The eddies exert minute stretching events on the vortex in a very rapid, apparently random, succession. This is associated with a series of slight random displacements of the vortex in the measurement plane. We may think of the vortex doing random steps to the sides, the step length being a function of the external fluctuation level and the internal resistance. On account of the scale separation, the vortex behaves like an integrator summing up the sequence of minute random events. While we cannot resolve every single step, the piled-up effect of very many random steps becomes visible at the macroscopic level and manifests in the form of meandering.

Brownian motion, as the prototype of a diffusion dynamics, is principally consistent with (1)–(2). Surprisingly, Gaussian distribution (1) of the meandering motion has received very little attention besides its use in the correction technique devised by [19] but can be understood straightforwardly in the proposed framework. By our above qualitative model, meandering can be seen as a random walk where the vortex does small steps to the left or to the right (say) at random. While we do not know the probability for a step to the left or right, we do know the probability to find the vortex in a certain location after it did very many steps. This is the essence of the central limit theorem, which guarantees convergence towards a Gaussian distribution irrespective of the probability to make a certain step. Probably the first application of the central limit theorem to turbulence is due to [46] to explain the Gaussian distribution in the final phase of decay and energy-containing eddies. The applicability is further discussed in [47–49].

3. Derivation of the model I: Kinematic-dynamic equivalence

The foregoing discussion suggests to consider the vortex-centre time series $t \mapsto X_i(t)$ as the central quantity determining meandering. As detailed in Section 2, we identify the canonical (wind-tunnel) experiment with a random experiment, the outcome of which is the realisation of one particular meandering trajectory $t \mapsto X_i^{(n)}(t)$. Running the (wind-tunnel) experiment over a certain measurement time N, is equivalent to repeating the same random experiment N times to yield an ensemble of meandering trajectories $\{t \mapsto X_i^{(n)}(t)\}_{n=0,\dots,N-1}$. As usual, we assume all trajectories to start off from the same initial condition (thus, a sure event) and only to diverge gradually. The corresponding (conditional) average is expressed as $\overline{(\cdot)}^{\boldsymbol{a}_0}$ if $\boldsymbol{a}_0$ denotes the initial state. A detailed discussion is postponed to Section 4.

3.1. Characterisation of the meandering motion in terms of vorticity moments

Vorticity is generally not space filling but rather tends to concentrate in isolated patches. The experimental setting introduced in Section 2 guarantees the existence of one such coherent vortex, the vorticity of which diffuses radially at an almost viscous time scale [15,24]. We then assume a volume $M \supseteq V \sim \ell_V^2$ centred around the mean drift path (Section 2) such that the vorticity does not diffuse out of ∂V over the time scales of interest.

We assume that the vorticity is a random process, one realisation of which is given by $t \mapsto w_z^{(n)}(t) \in L^1_\rho(V) \cap L^2_\rho(V)$, which takes values in the space of (polynomially) ρ-weighted integral and square-integrable functions over the integration domain $V \subseteq M$. (The practical confinement of vorticity in V in experiments serves as a sufficient condition for the existence of all integrals.) We assume the Reynolds decomposition $w_z(t,\boldsymbol{x}) = \overline{w_z}^{\boldsymbol{a}_0}(\boldsymbol{x}) + w_z'(t,\boldsymbol{x})$ $(\boldsymbol{x} \in M)$ and that the mean is approximately axisymmetric.

The zeroth spatial moment of vorticity is the circulation $\Gamma := \int_V \mathrm{d}^2x\, \overline{w_z}^{\boldsymbol{a}_0}(t,\boldsymbol{x}) \approx \text{const}$ over the considered time interval (due to the above definition of V).[1] Formally identifying vorticity with a mass distribution, the circulation corresponds to the total mass of the vortex (particle) contained in V. A dynamics of vortex systems has been derived on the basis of this analogy by [50].

From measurements of the Eulerian vorticity field, we can compute the linear first-order spatial moment

$$(\mathbb{R}^2 \ni)\boldsymbol{X}(t) := \frac{1}{\Gamma}\int_V \mathrm{d}^2x\, \boldsymbol{x} w_z'(t,\boldsymbol{x}), \tag{3}$$

corresponding to the centre of 'mass' of the vorticity patch V. We call $\boldsymbol{X}(t)$ the vortex centre. Randomness of the vorticity implies that $\boldsymbol{X}(t)$ is a vector-valued random process. Since the integral in (3) is skew-symmetric (due to $\boldsymbol{x}$), the mean vorticity drops out and $\boldsymbol{X}(t)$ is a centred random process (fluctuation).

In order to characterise the meandering motion, define the vector-valued covariance matrix (an asterisk * denoting conjugate transpose)

$$\overline{\boldsymbol{X}(t)\boldsymbol{X}^*(t)}^{\boldsymbol{a}_0} = \frac{1}{\Gamma^2}\int_V \mathrm{d}^2x \int_V \mathrm{d}^2x'\, \boldsymbol{x}\boldsymbol{x}'^* \overline{w_z'(t,\boldsymbol{x})w_z'(t,\boldsymbol{x}')}^{\boldsymbol{a}_0}. \tag{4}$$

The vortex-centre covariance matrix (4) is amenable to the eigenvalue problem

$$\overline{\boldsymbol{X}(t)\boldsymbol{X}^*(t)}^{\boldsymbol{a}_0}\boldsymbol{v}(t) = \sigma^2(t)\boldsymbol{v}(t). \tag{5}$$

Symmetry of the covariance matrix guarantees real eigenvalues and orthogonal eigenvectors. Since the eigenvectors can always be normalised to unity, their time dependence (if any) amounts to a mere rotation between different measurement planes.

Denoting x_1, x_2 the coordinates along the principal axes of $\boldsymbol{X}(t)$, the components $X_1(t), X_2(t)$ are uncorrelated and the covariance matrix $\overline{\boldsymbol{X}(t)\boldsymbol{X}^*(t)}^{\boldsymbol{a}_0}$ has diagonal form. Representation in the principal axes decouples the covariance matrix and each variance can be considered independently $(i = 1, 2)$

$$\sigma_i^2(t) := \overline{X_i^2}^{\boldsymbol{a}_0}(t) = \int_V \mathrm{d}^2x \int_V \mathrm{d}^2x'\, x_i x_i' \overline{w_z'(t,\boldsymbol{x})w_z'(t,\boldsymbol{x}')}^{\boldsymbol{a}_0}. \tag{6}$$

The standard deviation (6) is called meandering amplitude. According to (6), the meandering amplitude is equivalent to the linearly weighted integral over the two-point vorticity correlations in V at one time.

3.2. Development of the vorticity field in Karhunen–Loève modes

Recall from above, that $w_z'(t) \in L^2(V)$, endowed with the inner product $(a,b)_{L^2(V)} := \int_V \mathrm{d}^2x\, a(\boldsymbol{x})b(\boldsymbol{x})$ and induced norm $\|a\|^2_{L^2(V)} := (a,a)_{L^2(V)}$ for $a, b \in L^2(V)$ [51]. Since the space of square-integrable functions is separable [51], we can assume an expansion of the vorticity fluctuation into the series

$$w_z'(t,\boldsymbol{x}) = \sum_{i=1}^{\infty} c_i(t)\phi_i(t,\boldsymbol{x}), \tag{7}$$

that is, a linear combination of the random process $t \mapsto w_z'(t)$ for any given t into deterministic spatial patterns $\boldsymbol{x} \mapsto \phi_i(t,\boldsymbol{x})$ on V superposed at random according to the expansion coefficients $c_i(t) := (w_z'(t), \phi_i(t))_{L^2(V)}$.

Our previous analysis reveals that we are mainly interested in the second-order statistics of the vorticity. The optimal representation of the variance among all possible linear expansions is in terms of the Karhunen–Loève (KL) decomposition. For this reason, we take the modes ϕ_i in (7) as defined by a KL decomposition of the vorticity [32,47,52]; that is,

$$\int_V \mathrm{d}^2x'\, \overline{w_z'(t,\boldsymbol{x})w_z'(t,\boldsymbol{x}')}^{\boldsymbol{a}_0}\phi(t,\boldsymbol{x}') = \lambda(t)\phi(t,\boldsymbol{x}) \tag{8}$$

[1] Since the integral is even, the bulk contribution to the circulation automatically comes from the mean.

such that

$$(\phi_i(t), \phi_j(t))_{L^2(V)} = \delta_{ij} \tag{9}$$

and

$$\overline{c_i}^{\boldsymbol{a}_0}(t) = 0, \quad \overline{c_i(t)c_j(t)}^{\boldsymbol{a}_0} = \lambda_i(t)\delta_{ij} \tag{10}$$

as a consequence of Hilbert–Schmidt theory [51]. In (9)–(10) we see a double orthogonality; namely, deterministic orthogonality with respect to the $L^2(V)$-inner product holds for the eigenfunctions $\phi_i(t)$, while the expansion coefficients are stochastically orthogonal (uncorrelated). The eigenvalues $\lambda_i(t) = \overline{c_i^2}^{\boldsymbol{a}_0}(t)$ are real-valued and non-negative; we therefore assume them to be ordered in a decreasing sequence $\lambda_1(t) \geq \lambda_2(t) \geq \cdots \geq 0$ in terms of their contribution to the variance.

For the eigenfunctions (or KL modes), the same remark as above for the eigenvectors of the vortex-centre covariance matrix (5) applies. That is, for different times t, the eigenfunctions (of interest) only differ by a mutual rotation. The leading eigenfunctions are shown in Fig. 2 for the last measurement plane of the experiment discussed in Section 5. The pattern is structurally identical (up to a rotation) for all measurement planes in the experiment (not shown) in agreement with all previous findings discussed in Section 1.

In other words, the KL mode $\phi_i(t, \boldsymbol{x})$ describes a volumetric pattern in the three-dimensional flow domain as a downstream succession of dipolar structures shown in Fig. 2 subject to a gradual mutual rotation. Due to current limitations in the downstream resolution of experiments, t only takes values in a small and rather coarsely sampled interval, so that we possess only of a small number of spatial snapshots (five measurement planes at $zc^{-1} \in \{2, 4, 12, 20, 26\}$ in the experiment of Section 5). Although principally compatible with the proclaimed $|m| = 1$ symmetry (cf. Section 1), we cannot give a definite conclusion. Actually, the KL modes in the five measurement planes turn out to have very similar orientation almost aligned with the x, y axes. We therefore agree to suppress explicit dependence of the ϕ_i on t in the following.

Inserting expansion (8) into the covariance function (4) we get

$$\overline{\boldsymbol{X}(t)\boldsymbol{X}^*(t)}^{\boldsymbol{a}_0} = \frac{1}{\Gamma^2}\int_V \mathrm{d}^2x \int_V \mathrm{d}^2x' \, \boldsymbol{x}\boldsymbol{x}'^* [\overline{c_1^2}^{\boldsymbol{a}_0}(t)\phi_1(\boldsymbol{x})\phi_1(\boldsymbol{x}') + \overline{c_2^2}^{\boldsymbol{a}_0}(t)\phi_2(\boldsymbol{x})\phi_2(\boldsymbol{x}') + \cdots]$$

on account of the mutual uncorrelatedness of the expansion coefficients (10).

The leading KL modes have a dipole pattern, mutually rotate by $\pi/2$, thus aligned with the eigendirections of the vortex-centre covariance matrix (Fig. 2). As introduced above, let x_1 and x_2 be the coordinates in the directions of $\boldsymbol{v}_1$ and $\boldsymbol{v}_2$, respectively. We then see from Fig. 2 that the first KL mode ϕ_1 is an odd function of x_1 and an even function of x_2 around the centre, while it is the opposite for the second KL mode ϕ_2. On account of this symmetry, in the principal axes of $\boldsymbol{X}(t)$ thus holds

$$\begin{aligned}\overline{X_i^2}^{\boldsymbol{a}_0}(t) &= \frac{1}{\Gamma^2}\int_V \mathrm{d}^2x \int_V \mathrm{d}^2x' \, x_i x_i' \sum_{j=1}^{\infty} \overline{c_j^2}^{\boldsymbol{a}_0}(t)\phi_j(\boldsymbol{x})\phi_j(\boldsymbol{x}') = \\ &= \frac{\overline{c_i^2}^{\boldsymbol{a}_0}(t)}{\Gamma^2}\int_V \mathrm{d}^2x \int_V \mathrm{d}^2x' \, x_i x_i' \phi_i(\boldsymbol{x})\phi_i(\boldsymbol{x}') + O(\overline{c_3^2}^{\boldsymbol{a}_0}(t))\end{aligned} \tag{11}$$

The analysis shows that the leading error can at most be of the order of the largest neglected KL eigenvalue $\lambda_3(t)$. However, the typically multipolar structure of the higher-order KL modes cause deformation of the vortex rather than displacement and should therefore contribute only insignificantly to vortex meandering [27,28]. The actual error is therefore most likely less than $O(\overline{c_3^2}^{\boldsymbol{a}_0}(t))$. Writing this error under the integral in (11), we see that it goes to zero as $\overline{c_3^2}^{\boldsymbol{a}_0}(t)/\overline{c_i^2}^{\boldsymbol{a}_0}(t) \to 0^+$ $(i = 1, 2)$, i.e. as the leading KL modes have a larger share of the variance. In experiments, we find that $\overline{c_3^2}^{\boldsymbol{a}_0}(t) \approx \text{const}$ for all t (i.e. over the downstream measurement range), while, as we show below, $\overline{c_1^2}^{\boldsymbol{a}_0}(t) \approx \overline{c_2^2}^{\boldsymbol{a}_0}(t) \sim t$, such that the error gradually looses importance at a linear rate.

The two spatial integrals in (11),

$$I_{ii} := \int_V \mathrm{d}^2x \int_V \mathrm{d}^2x' \, x_i x_i' \, \phi_i(\boldsymbol{x})\phi_i(\boldsymbol{x}') > 0 \quad (i = 1, 2),$$

are merely geometrical form factors of dimension $\sim \ell^4$. To see this, let us suppose in a first approximation that $\phi_1(x_1, x_2) = f(x_1)g(x_2) \sim \ell^{-1}[\sin\frac{2\pi x_1}{2\ell} \cos\frac{\pi x_2}{2\ell}]$ in a square of edge length 2ℓ and $\phi_1(x_1, x_2) = 0$ else (cf. Fig. 2). Integrating over a square V of edge length $2\ell_V$, $\ell_V \geq \ell$, we find $\|\phi_i\|_{L^2(V)} = 1$ and $\int_V \mathrm{d}^2x \, \phi_i(\boldsymbol{x}) = 0$, consistent with the normalisation (9) and the above remark that the leading KL modes do not contribute to the circulation. We can then compute the integral analytically using Fubini's theorem and integration by parts to obtain $I_{ii} \sim \left(\frac{8}{\pi^2}\right)^2 \ell^4 \sim \ell^4$ [51]. We maintain that evaluating the integral for any particular experimental result should follow this scaling up to a proportionality constant

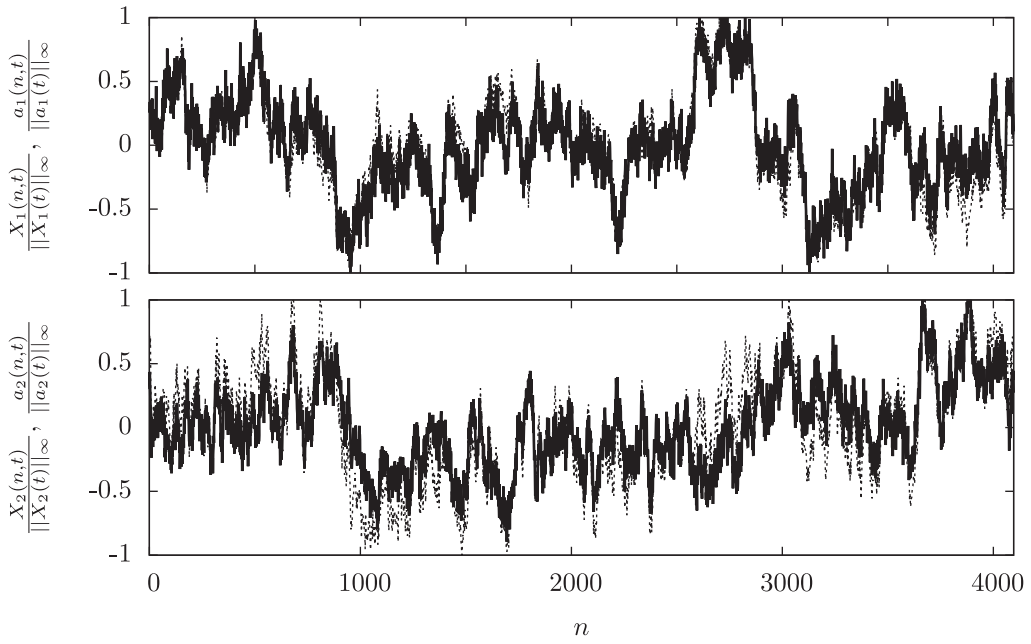

Fig. 3. Realisations (index n) of the vortex-centre position and of the leading vortex KL expansion coefficients for fixed evolution time $tt_a^{-1} = zc^{-1} = 26$.

$\Bbbk^2 > 0$ measuring the quality of the analytical approximation. (We expect that $\Bbbk \sim 1$ which we confirm in Section 5.) Thus, writing for the spatial integrals $I_{ii} = \Bbbk^2\ell^4$, it then follows for the two components

$$\overline{X_i^2}^{\boldsymbol{a}_0}(t) = I_{ii}\frac{\overline{c_i^2}^{\boldsymbol{a}_0}(t)}{\Gamma^2} \quad (i = 1, 2). \tag{12}$$

From (12), we see that $\overline{X_i^2}^{\boldsymbol{a}_0}(t) \sim \overline{c_i^2}^{\boldsymbol{a}_0}(t)$, $(i = 1, 2)$. That is, vortex meandering is the manifestation of what may be called a kinematic-dynamic duality as it describes at the same time the (material) vortex-centre motion in the fluid domain, while being equivalent to meandering in the phase space of the dynamics. This is further supported by directly comparing the measurement-time series (realisations) of $X_i(n, t)$ with $c_i(n, t)$ over $n \in [0, N-1]$ and for fixed t in Fig. 3 (data from the experiment of Section 5). The two curves clearly collapse (up to a constant scaling implied by (12)). We also note that the KL expansion coefficients that can be obtained from KL decomposition of the velocity field identically collapse (up to constant scaling) with the curves shown in Fig. 3. We conclude that the vorticity (enstrophy) and velocity (energy) dynamics are represented for the same mechanism and that these dynamics manifest in the kinematic motion of vortex meandering.

In passing we note that (12) indicates an efficient means for meandering correction. While a direct correspondence between meandering of the vortex centre $X_i(t)$ and the leading KL modes [27] and expansion coefficients $c_i(t)$ $(i = 1, 2)$ [28] has been speculated before, our above derivation leading to (12) establishes a definite proportionality for the first time to our knowledge. This implies that to leading order Eulerian fields can be corrected for vortex meandering by subtracting the leading two terms in the KL-expansion.

4. Derivation of the model II: Linear response theory of a Gauss–Markov process

We note that by (12), we have shifted the kinematic problem of finding the law governing $\overline{X_i^2}^{\boldsymbol{a}_0}(t)$ to the dynamics of an extensive state variable, namely $\overline{c_i^2}^{\boldsymbol{a}_0}(t) = \lambda_i(t)$ in V, i.e. the integral fluctuation enstrophy of the large scales. (Or integral fluctuation energy by the above observation.)

Unless otherwise stated, we assume Einstein's summation convention over repeated indices in what follows.

4.1. The phenomenological model: assumption of time-scale separation

Formally, the dynamics represented by $c_i(t)$ evolves in an infinite-dimensional phases space. However, we do not search to know the dynamics in all its details but rather are interested in a possibly small number of degrees of freedom associated with the dynamics of interest—vortex meandering in our case. Indeed, as we have seen in (11), the experimental

manifestation of meandering can (to leading order) be attributed to the dynamics of the leading KL mode pair. This suggests a dichotomy of the whole dynamical system $c_i(t)$ into a set of r resolved $\{a_i\}_{i=1,\dots,r}$ and u unresolved $\{b_i\}_{i=1,\dots,u}$ degrees of freedom, such that $\boldsymbol{c}(t) = (a_1, \dots, a_r, b_1, \dots, b_u)(t)$ and $r + u = m$ if m is the total number of degrees of freedom [37,53]. Taking the leading KL modes as the resolved dynamics is a typical and sensible choice, since they are usually associated with the slowest decay rates [54].

The particular interest of this dichotomy is perhaps best appreciated by considering the following abstraction of the experimental configuration. We suppose a fluid domain (the wind tunnel) of arbitrary lateral extension (stretching to infinity), in which one large-scale vortex is embedded into a surrounding fluid composed from a huge number of much smaller vortices (called eddies to make the distinction with the vortex) distributed at random. A similar model has been employed by [46] to model the dynamics of the energy-containing scales in turbulence. We assume the vorticity of the large vortex to be much larger than that of all other eddies. Recalling the formal analogy between vorticity and mass motivated in Section 3 [already suggested by 50], we obtain a problem similar to the encounter of a large, heavy planet with a large number of much smaller cosmological objects in an unbounded universe [40].

Let us suppose that the dynamics of the vortex is associated with the resolved scales $a_i(t)$, while we are lacking detailed knowledge about the dynamics of the surrounding eddies $b_i(t)$. Nevertheless, the large difference of the spatial scales and vorticity content suggests that the vortex and the surrounding eddies are associated with very different response time scales. We thus assume that

$$O\left(a_i\left(\frac{\mathrm{d}a_i}{\mathrm{d}t}\right)^{-1}\right) =: t_s \gg t_f := O\left(b_i\left(\frac{\mathrm{d}b_i}{\mathrm{d}t}\right)^{-1}\right), \tag{13}$$

meaning that $a_i(t)$ is a slow dynamics, while $b_i(t)$ constitutes a fast process. This means that we are interested in the slow, large-scale dynamics of a fluid volume concentrating almost all of vorticity, as it results from the integral, cumulative effect of a sequence of numerous minute excitations exerted by the surrounding fast, small-scale vorticity elements. Scale separation and the restriction to the large-scale dynamics by a Mori–Zwanzig projection is known as coarse graining [55–57]. The associated degrees of freedom are also called collective variables or order parameters [42].

4.2. Averaging

We understand wake-vortex dynamics as a random experiment with every experimental realisation labelled $n \in [0, N-1]$ ($N \to \infty$), drawn at random from an abstract sample space consisting of all admissible outcomes that are compatible with the boundary conditions. The realisation of the nth random experiment is the vector-valued random process $t \mapsto a_i^{(n)}(t)$ ($i = 1, 2, \dots, r$), where $a_i^{(n)}(t)$ is the actually measured state of the system in the nth repetition of the random experiment in the measurement plane defined by $t = \text{const}$. By definition, the random process $a_i(t)$ on $t \in [0, T]$ is completely determined if the distribution functions $p_{t_1,t_2,\dots,t_m}(\boldsymbol{a}_1, \boldsymbol{a}_2, \dots, \boldsymbol{a}_m)$ of $(\boldsymbol{a}_1, \boldsymbol{a}_2, \dots, \boldsymbol{a}_m) = (\boldsymbol{a}(t_1), \boldsymbol{a}(t_2), \dots, \boldsymbol{a}(t_m))$ for any m elements $t_1, t_2, \dots, t_m$ in $[0, T]$ are known [32,39]. The mean is defined by $\bar{a}_i(t) := \int_{-\infty}^{\infty} \mathrm{d}^r a\, a_i p_t(\boldsymbol{a})$ and does not depend on t if a_i is stationary. The two-point covariance is defined as $\overline{a_i(t_1)b_j(t_2)} := \int_{-\infty}^{\infty} \mathrm{d}^r a \int_{-\infty}^{\infty} \mathrm{d}^u b\, a_i b_j p_{t_1,t_2}(\boldsymbol{a}, \boldsymbol{b})$ and depends only on the time difference if a_i, b_j are stationary. (The variance is $\overline{a_i^2}(t) = \int_{-\infty}^{\infty} \mathrm{d}^r a\, a_i^2 p_t(\boldsymbol{a})$.) Higher multi-point moments depend on higher joint probability distributions.

Consideration of only the one-point statistics $p_t(\boldsymbol{a})$ completely describes a random process only if there is absolutely no correlation between subsequent elements of the sequence; that is, for a white-noise process. Markov processes are fully specified when all one- and two-point probability distributions are known, i.e. $p_t(\boldsymbol{a})$ and $p_{t_0,t_1}(\boldsymbol{a}_0, \boldsymbol{a}_1)$ or $p_t(\boldsymbol{a})$ and the conditional (transition) probability $p(t_1, \boldsymbol{a}_1 | t_0, \boldsymbol{a}_0)$ [39]. The conditional probability distribution $p(t, \boldsymbol{a}|\boldsymbol{a}_0)$ corresponds to repeating the same (random) experiment infinitely often, starting from the same identical initial condition $\boldsymbol{a}_0$. It will be convenient in the following analysis to consider in addition to $p(t, \boldsymbol{a}|\boldsymbol{a}_0)$ its two limiting probability distributions, that result from the limiting processes as $t \to 0^+$ and $t \to \infty$, respectively.

As a matter of fact, the random process of interest here is non-stationary for intermediate times. The associated probability density is governed by a partial differential equation which we find to be of Fokker–Planck type. Thus, the probability density $p(t, \boldsymbol{a} \mid \boldsymbol{a}_0)$ is the fundamental solution (Green's function) assuming the initial condition to be a sure event (viz. $p(t, \boldsymbol{a} \mid \boldsymbol{a}_0) \to \Pi_{i=1}^r \delta(a_i - a_{i,0})$ as $t \to 0^+$) [40,58]. We denote the mean of $\boldsymbol{a}(t)$ with respect to this probability distribution as

$$\overline{a_i}^{\boldsymbol{a}_0}(t) := \int \mathrm{d}^r a\, p(t, \boldsymbol{a} \mid \boldsymbol{a}_0) a_i \quad (i = 1, 2, \dots, r), \tag{14}$$

where integration extends over all of $\boldsymbol{a}$-space [53,59,60].

In order to introduce the short-time average, we anticipate that $a_i(t)$ represent the r coarse-grained variables, driven by u unresolved scales $b_i(t)$, which we assume to be stationary and rapidly fluctuating. Hence, it exists macroscopically infinitesimal time intervals over which $a_i = a_{i,0}$ while $b_i(t)$ runs over all possible states. This is known as the adiabatic approximation, which we can assume to hold for sufficiently short times after the initial condition [37,53]. We thus define

$$\overline{a_i}^{\boldsymbol{b}}(t) := \int \mathrm{d}^u b\, p(t, \boldsymbol{b} \mid \boldsymbol{a}_0) a_i \quad (i = 1, 2, \dots, r). \tag{15}$$

Eventually, noise-driven, linearly stable dynamics approaches an equilibrium state as $t \to \infty$. The corresponding probability distribution is stationary and equivalent to the Maxwell–Boltzmann distribution [60]. We write for averages taken with respect to the equilibrium distribution

$$\overline{a}_i^{\mathrm{eq}} := \int \mathrm{d}^r a \, p_{\mathrm{eq}}(\boldsymbol{a}) a_i \quad (i = 1, 2, \ldots, r), \tag{16}$$

which is independent of the initial condition.

4.3. Langevin equation: time-domain analysis

Irrespective whether c_i represents vorticity or velocity, the quadratic non-linearity of the Navier–Stokes equation implies that the dynamics is necessarily governed by a deterministic system of the type

$$\frac{\mathrm{d}c_i}{\mathrm{d}t} = -L_{ij}c_j + N_{ijk}c_j c_k, \quad c_i(0) = c_{i,0}. \tag{17}$$

By the above considerations, we split (17) into two sets of equations describing the dynamics in the slow a_i and fast b_i manifold, respectively. The two sets of equations form a coupled system by virtue of the non-linearity of (17). While the whole system (17) is intractable, restricting to the coarse-grained variables $a_i(t)$, we can appropriately formulate their dynamics in terms of a stochastic process where the fast scales $b_i(t)$ appear as random forcing [60]. Anticipating our below results, it is in fact this spatio-temporal coarse graining that leads to the Markov property of the resolved scales which behave like a diffusion process [56].

Thus, as is commonly done, identifying non-linearity with a stochastic forcing [5,36,61], (17) in the slow manifold reads[2]

$$\frac{\mathrm{d}a_i}{\mathrm{d}t} = -L_{ij}a_j + f_i, \quad a_i(0) = a_{i,0}, \tag{18}$$

where the initial condition is supposed to be a sure event imposed at a definite position in t ($t = 0$, say) [58]. By appeal to the scale separation (13), this is the Langevin equation describing the dynamics of an abstract Brownian particle [39]. We emphasise the crucially different nature of the two terms on the right-hand side, leading to competing contributions of (*i*) a stochastic forcing $f_i(t)$ that drives the dynamics out of equilibrium which is counteracted by (*ii*) a deterministic, stabilising 'linear friction' [4,38,42]. This latter contribution has been interpreted in terms of feedback that becomes activated as the dynamics is gradually driven away from the reference state by the random force [37]. Against the backdrop of (18), previous studies tried to explain meandering by concentrating on either one of the two terms. The theory of meandering being the consequence of a "passive beating about" of the vortex by free-stream disturbances is obtained by neglecting the stabilising effect of $L_{ij}a_j$. On the other hand, approaches to vortex dynamics by all kinds of linear instabilities follows from assuming f_i to be zero. We shall show in the following that experimental vortex meandering is in fact a competition between both effects. As far as we know, this point was first stressed by [45].

4.3.1. Short times $t < t_s$: Wiener process

In restricting to times $t < t_s$ which are short with respect to the slow vortex response time scale, no feedback ('friction') from the linear term in (18) is to be expected and the fluctuation dynamics is driven by the random forcing alone. In order to obtain the statistics of the coarse-grained, slow variables $a_i(t)$, we need to know the statistical properties of the forcing $f_i(t)$. We assume $f_i(t)$ to be stationary with zero mean $\overline{f_i}^{\boldsymbol{b}}(t) = 0$ and $\overline{f_i(s)f_j(t)}^{\boldsymbol{b}} = 2D_{ij}\delta(t-s)$, noting that the forcing becomes uncorrelated on the time scales of interest as a consequence of the scale separation (13) [39,40,59]. The solution to (18) follows from integrating from 0 to $t < t_s$, yielding

$$\Delta a_i(t) = a_i(t) - a_{i,0} = -\int_0^t \mathrm{d}s \, L_{ij}a_j(s) + \int_0^t \mathrm{d}s f_i(s) = -L_{ij}a_{j,0}t + \int_0^t \mathrm{d}s f_i(s), \tag{19}$$

since the slow variables $a_i(t)$ do not change appreciably over time (adiabatic approximation, slaving principle; [42]). Splitting the deviation from the initial condition $\Delta a_i(t) = \overline{\Delta a_i}^{\boldsymbol{b}}(t) + \Delta a_i'(t)$ into mean and fluctuation, it follows from (19) that

$$\overline{\Delta a_i}^{\boldsymbol{b}}(t) = \overline{a}_i^{\boldsymbol{b}}(t) - a_{i,0} = -L_{ij}a_{j,0}t, \tag{20}$$

$$\Delta a_i'(t) = a_i'(t) = \int_0^t \mathrm{d}s f_i(s). \tag{21}$$

We recall that the initial condition $a_{i,0}$ is known with certainty [58]. In (21) we recognise the kinematic problem of a passive particle suspended and dispersing in a fluid as studied by [25]. From this, we could in fact directly infer the statistical properties of $a_i(t)$ and $f_i(t)$ in the time range $t_f < t < t_s$. On account of the time-scale separation (13), there

[2] It is well known that (18) has to be understood in a generalised sense since $f_i(t)$ is no regular function [32].

always exists an intermediate time Δt for which the double limiting process $t_f \ll \Delta t \ll t_s$ holds; we say that Δt is at the same time microscopically large while it is macroscopically small [40]. With this, we write (21) as

$$a_i'(t) = \int_0^t \mathrm{d}s\, f_i(s) = \sum_{k=1}^{K} \int_{(k-1)\Delta t}^{k\Delta t} \mathrm{d}s\, f_i(s) = \sum_{k=1}^{K} \mathrm{d}B_i(\Delta t) \tag{22}$$

and note that (22) reduces the continuous problem to a succession of discrete increments or steps, viz. a random walk [40,62].

The scale separation implies that on the time scale of analysis, the strongly fluctuating process $f_i(t)$ has asymptotically vanishing correlation $t_f \ll \Delta t$ (as $\Delta t \to \infty$) and therefore can be idealised as a white-noise process. Vortex meandering therewith becomes the integral response to a stationary white-noise process modelling external forcing by a great number of minute excitations. The integral of an uncorrelated stationary random process is a non-stationary random process with stationary and uncorrelated increments [32].

Since $f_i(t)$ is a strongly fluctuating process with correlation time $t_f \ll \Delta t$, exerting numerous minute stretching events that destroy any correlation, subsequent increments in the series (22) tend to be stochastically independent (as $\Delta t \to \infty$) and the response process becomes memoryless [48,62]. Stationarity of $f_i(t)$ suggests to consider each small-scale forcing event as identically distributed [32,48]. Finally, from $\Delta t \ll t$ and $t = K\,\Delta t$ we conclude that $K \gg 1$. That is, the slow response variation $a_i'(t)$ is the sum of a large number of identically distributed, stochastically independent random excitations. (Each step $\mathrm{d}B_i(\Delta t)$ in the random walk (22) is the (in principle) experimentally observed net result of very many minute variations, e.g. random microscopic stretching events.) These are the requirements for the central limit theorem to apply. We thus conclude that each increment $\mathrm{d}B_i(\Delta t) \sim \mathcal{N}(0, 2\boldsymbol{D}\Delta t)$ and also the whole response process $a_i'(t) \sim \mathcal{N}(0, 2\boldsymbol{D}t)$ are normally distributed [40,56,62].

We therefore find in vortex meandering a manifestation of the central limit theorem, telling us that the piled-up response of a linear system driven by a statistically stationary forcing consisting of a large number of statistically independent excitations becomes Gaussian. It is important to note that this result is true independent of the detailed statistical structure of the forcing process and therefore does not depend on the particular experimental setup.

The covariance matrix is given by [25,59]

$$\overline{a_i' a_j'}^{\boldsymbol{b}}(t) = 2D_{ij}t \quad \text{where} \quad D_{ij} \coloneqq \frac{1}{2}\int_{-\infty}^{\infty} \mathrm{d}\tau\, \overline{f_i(t+\tau) f_j(t)}^{\boldsymbol{b}}. \tag{23}$$

A process $a_i'(t)$ is called Brownian-motion or Wiener process if it has independent Gaussian increments satisfying $\overline{a_i'(t) - a_i'(s)}^{\boldsymbol{b}} = 0$ and $\overline{(a_i'(t) - a_i'(s))^2}^{\boldsymbol{b}} = 2D_{ii}|t-s|$ for all $t_f \ll s < t \ll t_f$. This is equivalent to say that $a_i'(t)$ is Gaussian with independent increments. Independent increments are sufficient for a process to be memoryless, so that $a_i'(t)$ is Markovian [32,52,62].

4.3.2. Arbitrary times $t \geq O(t_s)$: Ornstein–Uhlenbeck process

As shown above, the forcing is a Gaussian random process characterised by the following stochastic moments,

$$\overline{f_i}^{\boldsymbol{a}_0}(t) = 0 \quad \text{and} \quad \overline{f_i(s) f_j(t)}^{\boldsymbol{a}_0} = 2D_{ij}\delta(t-s),$$

where D_{ij} symmetric, non-negative [53,57,59].

In going to evolution times t of the order of $O(t_s)$ and beyond, we have to account for the instationarity of the process $a_i(t)$. By virtue of (22), the general solution of (18) reads [40,59]

$$\boldsymbol{a}(t) - e^{-t\boldsymbol{L}}\boldsymbol{a}_0 = \int_0^t \mathrm{d}\tau\, e^{-(t-\tau)\boldsymbol{L}}\boldsymbol{f}(\tau) = e^{-t\boldsymbol{L}}\int_0^t \mathrm{d}\tau\, e^{\tau\boldsymbol{L}}\boldsymbol{f}(\tau) = e^{-t\boldsymbol{L}}\int_0^t e^{\tau\boldsymbol{L}}\mathrm{d}\boldsymbol{B}(\tau), \tag{24}$$

which is true whatever $t \geq 0$. The matrix exponential is defined in [63]. As shown in Section 4.3.1, $\mathrm{d}B_i(t)$ is a Wiener process of strength $2D_i$. It is well known that the response $a_i(t)$ for arbitrary time then is an Ornstein–Uhlenbeck process [59].

Consider the average over an ensemble of trajectories (24) all started from the identical initial condition. The mean of the slow scales evolves as

$$\overline{\boldsymbol{a}}^{\boldsymbol{a}_0}(t) = e^{-t\boldsymbol{L}}\boldsymbol{a}_0 \quad \forall t \geq 0, \tag{25}$$

recalling that $a_{i,0}$ is a sure event. Expanding the propagator into a Taylor series $e^{-t\boldsymbol{L}} = \mathbf{1} - t\boldsymbol{L} + O(t^2)$ $(t \to 0^+)$, where $\mathbf{1}$ is the identity matrix, it is readily seen that (20) follows as the short-time asymptotic from (25) in the limit as $t t_s^{-1} \to 0$. This was precisely our requirement in Section 4.3.1. Asymptotic stability of $\boldsymbol{L}$ further implies that $\overline{\boldsymbol{a}}^{\boldsymbol{a}_0}(t) \to 0$ as $t \to \infty$; this is consistent with the expectation that in the equilibrium distribution $\overline{\boldsymbol{a}}^{\mathrm{eq}} = 0$ [60]. The trivial case that $a_{i,0} = 0$ implies that $\overline{a_i}^{\boldsymbol{a}_0}(t) = 0$ for all $t > 0$ and $\overline{a_i}^{\mathrm{eq}} = 0$ by (25). In the general case, we deduce directly from (25) that the fluctuation around the mean, $\boldsymbol{\alpha}(t) = \boldsymbol{a}(t) - \overline{\boldsymbol{a}}^{\boldsymbol{a}_0}(t) = \boldsymbol{a}(t) - e^{-t\boldsymbol{L}}\boldsymbol{a}_0$, is identical to the particular part of the general solution (24). The covariance matrix of the Ornstein–Uhlenbeck process follows from (24) as

$$\boldsymbol{C}(t) \coloneqq \overline{\boldsymbol{\alpha}(t)\boldsymbol{\alpha}^*(t)}^{\boldsymbol{a}_0} = \int_0^t \mathrm{d}\tau \int_0^t \mathrm{d}\tau'\, e^{(\tau-t)\boldsymbol{L}}\overline{\boldsymbol{f}(\tau)\boldsymbol{f}^*(\tau')}^{\boldsymbol{a}_0} e^{(\tau'-t)\boldsymbol{L}^*} = 2\int_0^t \mathrm{d}\tau\, e^{(\tau-t)\boldsymbol{L}}\boldsymbol{D}e^{(\tau-t)\boldsymbol{L}^*}.$$

The evolution equation for the covariance matrix is readily derived from differentiating the covariance matrix with respect to t and applying Leibniz' rule of parametric integrals

$$\frac{\mathrm{d}\boldsymbol{C}(t)}{\mathrm{d}t} = 2\boldsymbol{D} - \boldsymbol{L}\boldsymbol{C}(t) - \boldsymbol{C}(t)\boldsymbol{L}^*, \quad \boldsymbol{C}(0) = 0, \tag{26}$$

and has the general solution

$$\boldsymbol{C}(t) = \boldsymbol{C}_{\mathrm{eq}} - e^{-t\boldsymbol{L}}\boldsymbol{C}_{\mathrm{eq}}e^{-t\boldsymbol{L}^*} \quad \forall t \geq 0, \tag{27}$$

which is actually the vector-valued generalisation of the variance of the scalar Ornstein–Uhlenbeck process for general $\boldsymbol{L}$. Herein, $\boldsymbol{C}_{\mathrm{eq}}$ denotes the covariance of $\alpha_i(t)$ for the equilibrium distribution,

$$\boldsymbol{C}_{\mathrm{eq}} := \overline{\boldsymbol{\alpha}\boldsymbol{\alpha}^*}^{\mathrm{eq}} = 2\int_0^\infty \mathrm{d}t\, e^{-t\boldsymbol{L}}\boldsymbol{D}e^{-t\boldsymbol{L}^*} = \boldsymbol{C}(t\to\infty), \tag{28}$$

that must be attained in the limit as $t \to \infty$ [57]. According to the equipartition theorem, in equilibrium the variance (e.g. fluctuation kinetic energy) must become equally distributed over all degrees of freedom; that is, $\boldsymbol{C}_{\mathrm{eq}} \sim u^2\boldsymbol{1}$ or component-wise $\overline{\alpha_i^2}^{\mathrm{eq}} \sim u^2$ for all i [59].

Since $\alpha_i(t)$ is stationary in equilibrium, $\boldsymbol{C}(t\to\infty) = \boldsymbol{C}_{\mathrm{eq}}$ must be independent of time and (26) becomes

$$\boldsymbol{L}\boldsymbol{C}_{\mathrm{eq}} + \boldsymbol{C}_{\mathrm{eq}}\boldsymbol{L}^* = 2\boldsymbol{D}. \tag{29}$$

This result can alternatively be derived directly from (28). Eq. (29) is known as the fluctuation–dissipation theorem [57] or generalised Einstein relation [53] and expresses a fundamental relation between the stochastic and systematic part of the driving force [56]. The left-hand side of (29) is symmetric by construction, although $\boldsymbol{L}$ is in general not. Decomposing $\boldsymbol{L} = \boldsymbol{S} + \boldsymbol{W}$, $\boldsymbol{S} = \boldsymbol{S}^*$ and $\boldsymbol{W} = -\boldsymbol{W}^*$, in (29) yields

$$\boldsymbol{S}\boldsymbol{C}_{\mathrm{eq}} + \boldsymbol{C}_{\mathrm{eq}}\boldsymbol{S} = 2\boldsymbol{D} \quad \to \quad \boldsymbol{S}\boldsymbol{C}_{\mathrm{eq}} = \boldsymbol{C}_{\mathrm{eq}}\boldsymbol{S} = \boldsymbol{D}, \tag{30}$$

$$[\boldsymbol{W}, \boldsymbol{C}_{\mathrm{eq}}] := \boldsymbol{W}\boldsymbol{C}_{\mathrm{eq}} - \boldsymbol{C}_{\mathrm{eq}}\boldsymbol{W} = 0. \tag{31}$$

Symmetry of $\boldsymbol{D}$ implies symmetry of $\boldsymbol{S}\boldsymbol{C}_{\mathrm{eq}}$, which is a form of Onsager's reciprocal relations [53,57].

We recall that we do not assume any particular symmetry of L_{ij}, in particular, $[\boldsymbol{L}, \boldsymbol{L}^*] := \boldsymbol{L}\boldsymbol{L}^* - \boldsymbol{L}^*\boldsymbol{L} \neq 0$ in the linear dynamics of coherent line vortices [20,36]. This seems to preclude any further simplification of the equations beyond this point. In particular, $\boldsymbol{L}$ is not orthogonally diagonalisable such that we must expect all degrees of freedom to be linearly coupled. Stochastic-forcing analysis thus progresses by computing the KL decomposition of (28) [21,64].

We would like to make the analogy with the Ornstein–Uhlenbeck variance of scalar Brownian motion more explicit. However, the essential difficulty encountered here is that, since $\boldsymbol{L}$ and $\boldsymbol{L}^*$ do not commute, $e^{t\boldsymbol{L}}e^{t\boldsymbol{L}^*} \neq e^{t(\boldsymbol{L}+\boldsymbol{L}^*)}$ [63]. Rather than deriving the numerical value of the variance in any particular experiment at hand, our aim is to find an estimate for the general law governing the variance evolution of the coarse-grained variables which is valid for all experiments that are compatible with our assumptions.

Recall from Section 3 that, by construction, we work in the slow linear manifold spanned by the leading KL modes. In this representation, $\boldsymbol{C}(t) = \overline{\boldsymbol{\alpha}\boldsymbol{\alpha}^*}^{\boldsymbol{a}_0}(t)$ is diagonal with all entries $\overline{\alpha_i^2}^{\boldsymbol{a}_0}(t)$ being mutually uncorrelated. We maintain that this is true for all t and, in particular, also holds for the equilibrium covariance. This is consistent with the theoretical results of [21,36]. This means that (27) reads in index notation

$$\overline{\alpha_{(i)}^2}^{\boldsymbol{a}_0}(t)\delta_{ij} = \overline{\alpha_{(i)}^2}^{\mathrm{eq}}\delta_{ij} - e^{-tL_{ik}}\overline{\alpha_{(k)}^2}^{\mathrm{eq}}\delta_{kl}e^{-tL_{jl}} = \overline{\alpha_{(i)}^2}^{\mathrm{eq}}\delta_{ij} - \overline{\alpha_{(k)}^2}^{\mathrm{eq}}e^{-tL_{ik}}e^{-tL_{jk}},$$

where summation is not implied over indices in parentheses. We recognise in $e^{-t\boldsymbol{L}}e^{-t\boldsymbol{L}^*}$ the kernel of the controllability Gramian $\boldsymbol{C}_{\mathrm{eq}}$ used in stochastic-forcing approaches to derive a hierarchy of spatial structures as they contribute to the variance of the equilibrium state [64]. Likewise, recalling that the eigenvalue problem of $e^{-t\boldsymbol{L}^*}e^{-t\boldsymbol{L}}$ yields the optimal initial perturbation (for given $t > 0$), we note that the same analysis of $e^{-t\boldsymbol{L}}e^{-t\boldsymbol{L}^*}$ yields the corresponding perturbation at t. All previous studies known to the author unanimously find a vortex response mode very similar in structure to those shown in Fig. 2 [see 20,21,36, and references therein]. This suggests that $e^{-t\boldsymbol{L}}e^{-t\boldsymbol{L}^*}$ is (close to) diagonal in the coarse-grained coordinates.

By virtue of the equipartition theorem, assume that $\boldsymbol{C}_{\mathrm{eq}} \sim \left(\frac{u}{\ell}\right)^2 \ell^2\boldsymbol{1} \sim u^2\boldsymbol{1}$, so that

$$\overline{\alpha_{(i)}^2}^{\boldsymbol{a}_0}(t)\delta_{ij} = u^2\left[\delta_{ij} - e^{-tL_{ik}}e^{-tL_{jk}}\right].$$

Or equivalently in vector notation,

$$\boldsymbol{C}(t) = u^2\left[\boldsymbol{1} - e^{-t\boldsymbol{L}}e^{-t\boldsymbol{L}^*}\right] = u^2\left[\boldsymbol{1} - e^{-t(\boldsymbol{L}+\boldsymbol{L}^*)+\frac{t^2}{2}[\boldsymbol{L},\boldsymbol{L}^*]+\cdots}\right]. \tag{32}$$

The second identity of the matrix exponential holds even if $[\boldsymbol{L}, \boldsymbol{L}^*] \neq 0$ by the Baker–Campbell–Hausdorff formula. Even more, if $[\boldsymbol{L}, [\boldsymbol{L}, \boldsymbol{L}^*]] = [\boldsymbol{L}^*, [\boldsymbol{L}, \boldsymbol{L}^*]] = 0$ the argument in the exponential of (32) can exactly be truncated after the quadratic term [65]. Writing $2\boldsymbol{S} := \boldsymbol{L} + \boldsymbol{L}^*$, we expand the matrix exponential in a Taylor series to get

$$\boldsymbol{C}(t) = u^2[\boldsymbol{1} - (\boldsymbol{1} - 2t\boldsymbol{S} + O(t^2))] \approx 2u^2\boldsymbol{S}t. \tag{33}$$

We note that (33) is consistent in that $\boldsymbol{C}$ and $\boldsymbol{S}$ are both real, symmetric, non-negative definite (as a consequence of the (assumed) linear stability of vortex dynamics). For $\boldsymbol{C}(t)$ being diagonal, $\boldsymbol{S}$ is diagonal. We denote the ith diagonal element by s_i. This means that the linear vortex response, the KL modes shown in Fig. 2 and the eigenvectors of the strain-rate tensor are structurally similar. We thus obtain

$$\overline{\alpha_i^2}^{\boldsymbol{a}_0}(t) \sim 2u^2 s_i t \sim 2u^2 \frac{t}{t_s}, \tag{34}$$

where we recognise s_i^{-1} as the response time t_s of the slow variables.

4.4. Langevin equation: frequency–space analysis

Spectral analysis of vortex meandering is a commonly employed tool, which has been used frequently to characterise the dynamics. We give a brief account on some aspects of this analysis in the following.

Let there be given an experimental time series that we judge representative of the meandering motion. This choice is not obvious and past studies considered various different time series, partly motivated by limitations in the experimentally available data due to the measurement device. Studies using hot-wire measurements usually relied on the streamwise component of the fluctuation velocity in the mean vortex centre [13,19,30], while studies based on particle image velocimetry measurements commonly considered the leading KL expansion coefficients [28] or the vortex-centre position [16].

Whether the streamwise velocity in the mean vortex-centre position is fully representative of the meandering motion may be doubted and we have evidence that it is indeed incompatible with some of the fundamental meandering characteristics discussed above. For instance, the streamwise component of the fluctuation kinetic energy seems to decay with t (i.e. downstream) [13,30] and the spectral signature in the relevant range for meandering probably does not comply with the characteristic signature derived below. Some additional discussion on this topic can be found in [45].

In any event, we observe a remarkable universality of the spectral signature across all documented experiments. In particular, we note that the power spectra seem to scale with the turbulence intensity, while they are essentially independent of the characteristic scales of the free-stream turbulence. This fact is unanimously observed in experiments on vortex dynamics in grid turbulence [16,17,24,30]. Previous studies exclusively focused on describing the signature of the power spectra in the inertial range. From these analyses, we have considerable evidence that the power spectra obey a power-law decay roughly proportional to the third power of the frequency in the inertial range, which is reminiscent of two-dimensional turbulence [13,16,19,30]. However, it seems that no study so far addressed the spectral signature of the low-frequency range which is associated with the energy-carrying scales [48]. Our above analysis and the theory of Brownian motion suggest that it is precisely this range which is associated with the meandering motion. In the following, we derive the expected spectral signature of vortex meandering in this low-frequency range.

The theory of Brownian motion is tightly coupled with the development of harmonic analysis of random functions. As a matter of fact, a spectral representation in terms of a Fourier integral exists for every stationary random process [32,62]. We have seen above that $(n, t) \mapsto a_i(n, t)$ is not stationary in the evolution time t (in other words, on the downstream range z of interest), while it is stationary in the measurement time n. (This is a consequence of the initial condition [32,53].) Keeping t fixed (that is an Eulerian point of view in one measurement plane), we assume the following problem

$$\frac{\mathrm{d}\boldsymbol{a}_t}{\mathrm{d}n} = -\boldsymbol{L}\boldsymbol{a}_t + \boldsymbol{f}(n), \quad \boldsymbol{a}_t(n=0) = \int_{-\infty}^{0} \mathrm{d}m\, e^{m\boldsymbol{L}}\boldsymbol{f}(m). \tag{35}$$

This definition reflects our requirement that the solution has forgotten the initial condition and is stationary in n, viz.

$$\boldsymbol{a}_t(n) = \int_{-\infty}^{n} \mathrm{d}m\, e^{-(n-m)\boldsymbol{L}}\boldsymbol{f}(m).$$

This means that at $n = 0$ an equilibrium between forcing and vortex response dynamics has been reached.

In what follows, we consider the stationary, zero-mean sequence $\alpha_i(n, t = \text{const})$ in a fixed measurement plane $t = \text{const}$ and suppress t dependence if unambiguous. The covariance function is defined as $R_{ij}(\nu) := \overline{\alpha_i(n)\alpha_j(n+\nu)} = \lim_{N\to\infty} N^{-1} \sum_{n=0}^{N-1} \alpha_i(n)\alpha_j(n+\nu)$ in terms of the (discrete) time average. Due to stationarity we can always write $n = 0$ in the covariance function. According to a multi-dimensional generalisation of Khintchine's theorem [66], $R_{ij}(\nu)$ is the covariance function of a continuous, stationary random process if and only if

$$R_{ij}(\nu) = \int_{-\infty}^{\infty} e^{\mathrm{i}\omega\nu}\mathrm{d}G_{ij}(\omega) = \int_{-\infty}^{\infty} \mathrm{d}\omega\, G_{ij}(\omega)e^{\mathrm{i}\omega\nu}, \tag{36}$$

where the $\mathrm{d}G_{ij}(\omega)$ are of bounded variation in $\mathbb{R}$. The second equality holds if $R_{ij}(\nu) \to 0$ sufficiently rapidly as $|\nu| \to \infty$ to guarantee that $\int_{-\infty}^{\infty} \mathrm{d}\nu\, |R_{ij}(\nu)| < \infty$ [32]. The inverse transform reads

$$G_{ij}(\omega) = \frac{1}{2\pi} \int_{-\infty}^{\infty} \mathrm{d}\nu\, R_{ij}(\nu)e^{-\mathrm{i}\omega\nu}.$$

The covariance function for fluctuations about the equilibrium falls of exponentially as

$$\boldsymbol{R}(\nu) = e^{-|\nu|\boldsymbol{L}}\boldsymbol{R}(0), \tag{37}$$

as follows from (35) upon multiplication by $a_i(n=0)$ (stationarity), subsequent averaging and recalling that $a_i(n=0)$ is a random variable, too [53].

The forcing power spectrum is $\overline{\hat{f}_i(\omega)\hat{f}_j(\omega')} = F_{ij}(\omega)\delta(\omega-\omega')$, where stochastic orthogonality between different Fourier modes (with zero mean) is necessary and sufficient for a stationary process [32]. For times long compared to the fast time scale t_f, or equivalently for $\omega t_f \ll 1$, we can approximate $F_{ij}(\omega) \to F_{ij}(0) = 2D_{ij}$ by a constant. This is the spectral signature of a white-noise process (cf. Section 4.3.1). Taking the Fourier transform of the Langevin equation (18) and its adjoint, the response power spectrum corresponding to (37) is readily shown to be

$$\boldsymbol{G}(\omega,\omega') := \overline{\hat{\boldsymbol{\alpha}}(\omega)\hat{\boldsymbol{\alpha}}^*(\omega')} = (\boldsymbol{L}+\mathrm{i}\omega)^{-1}\overline{\hat{\boldsymbol{f}}(\omega)\hat{\boldsymbol{f}}^*(\omega')}(\boldsymbol{L}^*-\mathrm{i}\omega')^{-1} = (\boldsymbol{L}+\mathrm{i}\omega)^{-1}2\boldsymbol{D}(\boldsymbol{L}^*-\mathrm{i}\omega)^{-1}, \tag{38}$$

since the forcing has asymptotically white-noise spectrum on the time scales of interest. If we assume that $D_{ij} \sim D\delta_{ij}$ and that we can find a single response time scale $t_s = \lambda^{-1}$ for $\boldsymbol{L}$, (38) simplifies to

$$G(\omega) = \frac{2D}{(\lambda+\mathrm{i}\omega)(\lambda-\mathrm{i}\omega)} = \frac{2D}{\lambda^2+\omega^2}, \tag{39}$$

which is the spectral signature of the stationary Ornstein–Uhlenbeck process for fluctuations about the equilibrium [32, 62]. For $\lambda \to 0$, that is for infinitely slow response time $t_s \to \infty$, we readily see from (39) that $G(\omega) \xrightarrow{\lambda\to 0} F(0)\omega^{-2}$ $(\omega \neq 0)$, which is the response power spectrum of the Wiener process. Assuming $F(0) < \infty$, this implies that $G(\omega) \to \infty$ as $\omega \to 0$ if $\lambda \to 0$.

Alternatively, by direct computation of the Fourier transform of an exponentially-correlated stationary random process of variance A, we obtain $G(\omega) = \frac{A}{\pi}\frac{\lambda}{\lambda^2+\omega^2}$ [32]. Comparison between the different forms of the response power spectrum shows that $F(0) = 2D = \frac{A\lambda}{\pi}$. This shows again that the spectral signature of the forcing is directly related to the macroscopic diffusion constant, which is essentially the ratio of the fluctuation level A and the response time scale λ^{-1}.

5. Comparison with experiments of trailing vortices

We compare our theoretical results with an experimental database gathered in the F2 wind tunnel of the ONERA centre in Le Fauga-Mauzac. A detailed account of the experiment can be found in [34], the configuration being almost identical to the one described in [26]. Among the different configurations probed, the setting of interest here is the flow past a NACA 0012 wing of chord length $c = 0.125\,\mathrm{m}$ suspended on a rigid support structure from the tunnel roof at an angle of incidence of 9°. The inflow velocity being fixed at $U_\infty = 20\,\mathrm{m\,s^{-1}}$, yielding a chord-based Reynolds number $R_c := cU_\infty/\nu = 1.7\times10^5$. The turbulence intensity in the facility is $\mathit{u}U_\infty^{-1} \lesssim 5\times10^{-3}$ and the vortex-core radius, defined in Section 2, is $\ell_1 \approx 5\times10^{-3}\,\mathrm{m}$. This latter value agrees with previous findings of [19,24,26,31,67]. Fig. 2 suggests that $\ell c^{-1} \approx 0.1$, which is corroborated by the circulation characteristics discussed below.

Three-dimensional, high-speed stereo particle image velocimetry (PIV) measurements are taken in five measurement planes located at $zc^{-1} \in \{2, 4, 12, 20, 26\}$ at a sampling rate of $f_s = 3$ kHz. A totality of $N = 4096$ samples are thus recorded and the same experiment has been repeated in ten identically prepared runs.

The radial profile of the circulation increases monotonously, taking values in $\Gamma(r)/cU_\infty = 0.1\ldots0.3$ for $r = \ell_1\ldots\infty$. Monotony and range are in agreement with the findings of [19,24,26,31,67] for the same wing model, similar Reynolds number and angle of incidence. The circulation increases rapidly over $r = 0,\ldots,\ell$, where $\ell \approx 2\,\ell_1$ is the support radius, indicating that most of the vorticity is confined to this range [24,31]. According to Section 3, we take the integration volume V larger than this range of rapid change. Due to the much slower circulation increase outside the vortex support, this value of the circulation is rather insensitive to the particular size of the integration volume. We also note that the circulation profiles are practically constant over the measurement range as also found by [19]. As an order-of-magnitude estimate, we set $\Gamma/cU_\infty \sim 0.1$, which is a representative value for the present [34] and typical experiments (cf. Table A.2 in Appendix).

We conclude that all flow variables closely match previous findings and that the variance is consistent with the differences in the experimental parameters (e.g. Reynolds number, angle of incidence). We thus consider the present experiment as representative for the phenomenon under study.

From the experimental parameters, we derive the actual values of the time scales governing the dynamics. The result is resumed in Table 1. The slow response time scale t_s is the reciprocal of the eigenvalues s_i of the symmetric part $\boldsymbol{S}$ of the linear friction matrix $\boldsymbol{L}$ (to leading order). To get an idea of the governing dynamics, we recall that $\boldsymbol{L}$ has contributions from advection by the mean, vortex stretching or energy production by the mean-velocity gradient and viscous diffusion. In general, we can decompose $\boldsymbol{L} = \boldsymbol{S}+\boldsymbol{W}$, where the skew-symmetric part $\boldsymbol{W}$ contains advection and the skew-symmetric part of the mean-velocity gradient (rotation). The symmetric part comprises the symmetric part of the velocity gradient and viscous diffusion. For rotation-dominated flow at high Reynolds numbers, we expect two characteristic time scales, viz. the shear scale $t_s^{-1} \sim \nabla\bar{\boldsymbol{u}} + \nabla^*\bar{\boldsymbol{u}}$ governing growth or decay and the rotation scale $t_r^{-1} \sim \nabla\bar{\boldsymbol{u}} - \nabla^*\bar{\boldsymbol{u}}$ characteristic of conservative redistribution. In terms of experimentally measurable quantities, the rotation time scale is approximated by $t_r \approx 2\pi\ell_1^2/\Gamma$. Analysis of the spectra of the linearised Navier–Stokes operator around the Lamb–Oseen vortex suggest that t_s should be about two orders of magnitude larger than t_r, e.g. [35]. In general, $t_s = \kappa t_r$ for some $\kappa > 1$.

Table 1
Experimental time scales.

Time scale	Estimate
Advection time	$t_a := cU_\infty^{-1} = 6.25 \times 10^{-3}$ s
Rotation time	$t_r := 2\pi \ell_1^2 \Gamma^{-1} \approx 0.05\, cU_\infty^{-1} \approx 0.3 \times 10^{-3}$ s
Slow response time	$t_s = \kappa t_r \approx 10^2 t_r \approx 5\, cU_\infty^{-1} \approx 30 \times 10^{-3}$ s ($:= \lambda^{-1}$)

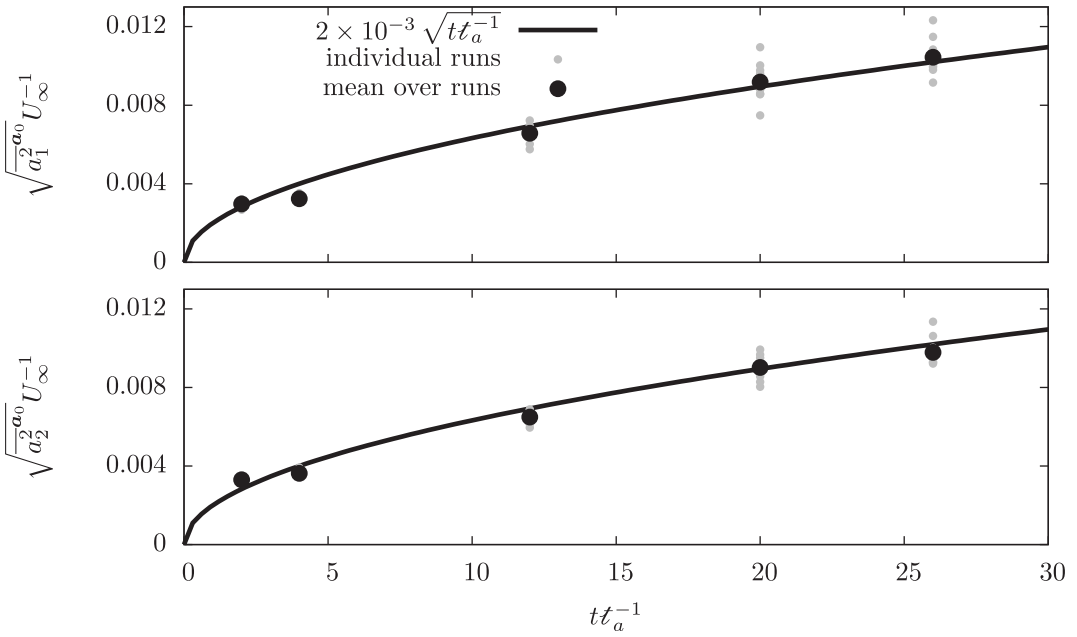

Fig. 4. Temporal (downstream) evolution of the square root of the two leading eigenvalues of the vorticity covariance function normalised on U_∞. Comparison of the different experimental runs (small grey dots), the arithmetic mean growth (large black dot) and the graph of the amplitude law (34) (thick line). A slight anisotropy of the order of $\pm O(10^{-4})$ in the experimental data has been corrected for by a corresponding scaling constant.

5.1. Vorticity fluctuations

In Section 4, the variance of the large-scale vorticity fluctuations was shown to obey (34). For the present experimental parameters and the response time scale given in Table 1, in particular using $uU_\infty^{-1} = 5 \times 10^{-3}$ and $s_i = 5^{-1}c^{-1}U_\infty$, we obtain

$$\frac{\overline{a_i^2}^{\boldsymbol{a}_0}(t)}{U_\infty^2} \sim \left(\frac{u}{U_\infty}\right)^2 s_i t \sim 25 \times 10^{-6} \frac{tU_\infty}{5c} \sim 5 \times 10^{-6} \frac{t}{t_a}.$$

A comparison of (34) with the experiment is shown in Fig. 4. We find a good agreement between the model (thick line) and the mean vorticity variance growth taken over all experimental runs (large black dots). The variance in each of the individual runs is shown by small grey dots. From (34), we have that $\overline{a_i^2}^{\boldsymbol{a}_0}(t = t_s) \sim u^2$, so that we expect the integral enstrophy level at about five chords from the origin to be of the same order of magnitude as the turbulence intensity squared; which is indeed the case in Fig. 4. This indicates that the vortex is in equilibrium with the surrounding at this point, which may serve as a fictitious starting point of the meandering experiment.

We also deduce from Fig. 4 that the slow variables a_i only slightly deviate from their initial value on average, which was the requirement of the adiabatic approximation in Section 4.3.1. As a first estimate, we note $(\sqrt{\overline{a_i^2}^{\boldsymbol{a}_0}}(25) - \sqrt{\overline{a_i^2}^{\boldsymbol{a}_0}}(5))/\sqrt{\overline{a_i^2}^{\boldsymbol{a}_0}}(5) \sim 1$.

We can further estimate the length scale ℓ of the large-scale vorticity from this finding. It is a well-known result due to G. I. Taylor that the local enstrophy in homogeneous isotropic turbulence at very high Reynolds number is of the order $\overline{w_z^2}^{\boldsymbol{a}_0} \sim \left(\frac{u}{\ell_T}\right)^2$, where u is the turbulence intensity (proportional to the amount of kinetic energy in the large-scale turbulence) and ℓ_T the Taylor microscale [33,46,48]. However, this scale estimate holds for the small, dissipative scales. The appropriate scales of the considered large-scale meandering motion should be the integral scale ℓ and u as before [4,6]. Since $\overline{a_i^2}^{\boldsymbol{a}_0}$ represents the integral enstrophy in V associated with KL mode ϕ_i, we expect that

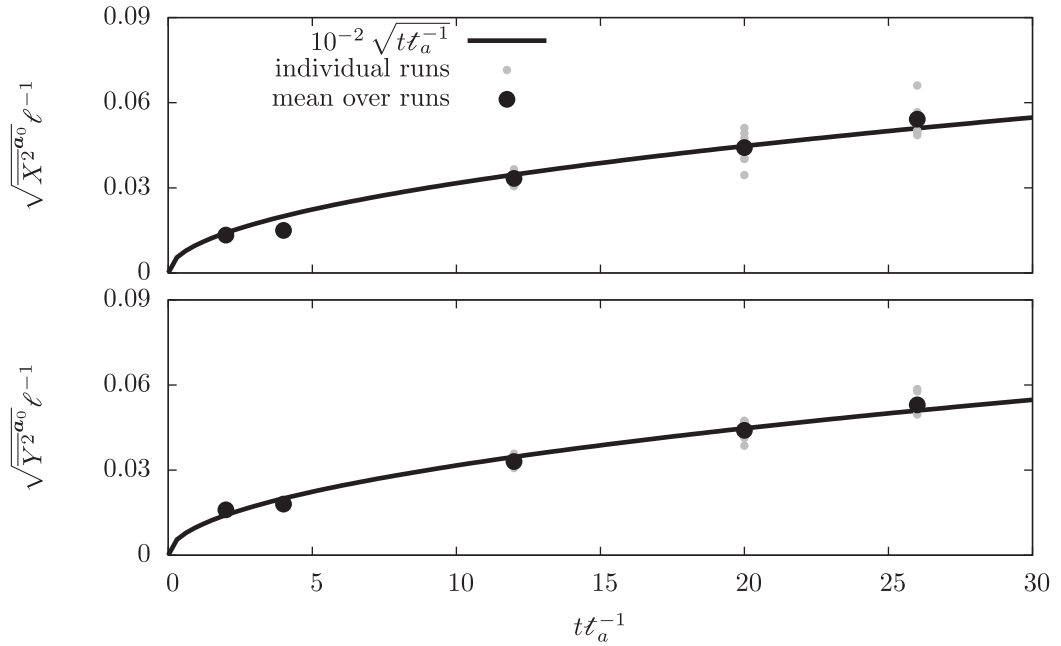

Fig. 5. Temporal (downstream) evolution of the spanwise and vertical meandering amplitude normalised on ℓ. Comparison of the different experimental runs (small grey dots), the arithmetic mean growth (large black dot) and the graph of the amplitude law (40) (thick line). A slight anisotropy of the order of $\pm O(10^{-3})$ in the experimental data has been corrected for by a corresponding scaling constant.

$\overline{a_i^2}^{a_0} \sim \ell^2 \left(\frac{u}{\ell}\right)^2 \sim u^2$ on account of the (practically) compact-support argument of Section 3. This is consistent with our model and the experimental results.

In Section 3, we argued that the leading contributions to the fluctuation velocity variability obey the same meandering signature as the vorticity. At this point, let us merely mention that the leading two eigenvalues of the velocity covariance function follow a qualitatively identically behaviour as is shown in Fig. 4.

5.2. Meandering amplitude

The scaling law of the meandering amplitude follows from combining (12) with (34) as

$$\frac{\overline{X_i^2}^{a_0}(t)}{\ell^2} \sim \left[2k^2\frac{\ell^2}{\Gamma^2}\right] u^2 s_i t \quad (i=1,2),$$

where the term in brackets is the proportionality constant between meandering in phase and physical space. We see that the length of one step in the random walk is proportional to the turbulence intensity u, while it is reciprocally dependent on the vortex resistance Γ. The term in brackets is estimated using $\Gamma/cU_\infty \sim 10^{-1}$, $\ell c^{-1} \sim 10^{-1}$ as introduced above and $k \sim \pi$ in agreement with our remark in Section 3. This yields the scaling law of the meandering amplitude

$$\frac{\sqrt{\overline{X_i^2}^{a_0}}(t)}{\ell} \sim 10^{-2}\sqrt{\frac{t}{t_a}} \quad (i=1,2). \tag{40}$$

A comparison between the meandering amplitudes in the experiment with the model law (40) is shown in Fig. 5 using the same line and point styles as in Fig. 4 for the vorticity variance.

The bivariate frequency distribution of the vortex-centre position is shown in Fig. 6 for the last measurement plane and over all runs. Histograms of the respective marginal probability densities are well approximated by Gaussian distributions (cf. Section 4). The probability to find the vortex centre in $[x_i, x_i + \mathrm{d}x_i\,]$ obeys a bivariate Gaussian distribution in all other measurement planes, too. Decreasing standard deviation (meandering amplitude) as we approach the wing according to (40) implies progressively narrowing probability densities. This is indeed the case and consistent with Fig. 5 (not shown). Downstream widening probability densities are also reported in [17,23,31].

Rather than searching for the probability of finding the vortex in an interval $\mathrm{d}x_i$ around a definite point x_i, it may be more interesting to know the probability with which the vortex is in a certain radial annulus $[r, r + \mathrm{d}r\,]$ from the mean position. This is the original question of the random walk due to K. Pearson (1905, Nature), solved in a reply by Lord

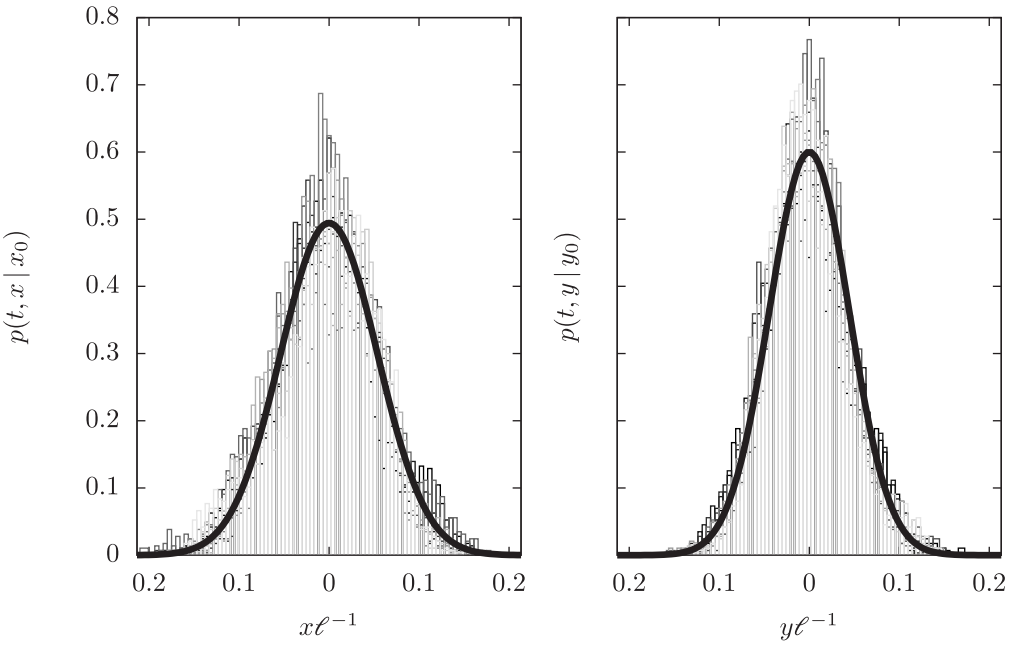

Fig. 6. Marginal frequency distributions of the spanwise and vertical vortex-centre position in the last measurement plane. Histograms of individual runs (different grey shadings) and the fit of the mean over the runs to a Gaussian probability density (thick line).

Rayleigh [40]. If X_i is normally distributed, the norm (or radius coordinate) of the vortex-centre position must consequently be Rayleigh-distributed, viz. $R := \|\boldsymbol{X}\| \sim \mathcal{R}(\sigma)$. The probability density of the Rayleigh distribution reads

$$p(r)\mathrm{d}r = \frac{r}{\sigma^2} e^{-\frac{r^2}{2\sigma^2}} \mathrm{d}r \quad \forall r \geq 0, \tag{41}$$

with the scale parameter $\sigma^2 = \frac{2}{4-\pi} \operatorname{Var} R$ in terms of the variance $\operatorname{Var} R$ of the radius coordinate [32]. Fig. 7 shows that the frequency distributions obtained for the individual runs in the last measurement plane are indeed well approximated on average by the Rayleigh probability density (41).

In Section 4.4, we have derived the simplified signature of the meandering motion as an Ornstein–Uhlenbeck process in the equilibrium limit. Assuming that the dynamics can be identified with one response time scale $t_s = \lambda^{-1}$, we recall that the result can be expressed equivalently in (measurement-)time domain in terms of the autocorrelation function (cf. (37))

$$\frac{R_{ii}(\nu; t)}{R_{ii}(0; t)} = e^{-\lambda|\nu|}, \quad t_s = \lambda^{-1}, \tag{42}$$

or (see (39)) as the response power spectrum in frequency domain ($A(t) := R_{ii}(0; t)$ is the local variance in t)

$$G(\omega; t) = \frac{A(t)}{\pi} \frac{\lambda}{\lambda^2 + \omega^2} = \frac{F(0; t)}{\lambda^2 + \omega^2},$$

where in each case the measurement plane t is kept fixed [32]. Using λ as given in Table 1 and for the variance in the last measurement plane $A(t)\ell^{-2} \sim 25 \times 10^{-4}$ (from (40) and Fig. 5), we estimate

$$G(\omega; t t_a^{-1} = 26) \frac{U_\infty}{\ell^2 c} \sim \frac{2 \times 10^{-4}}{\lambda^2 + \omega^2} \quad \text{where} \quad F(0; t) = \frac{A(t)\lambda}{\pi} \sim 2 \times 10^{-4} \frac{\ell^2 U_\infty}{c}. \tag{43}$$

Fig. 8 shows a comparison between the theoretical model (42)–(43) and the experiment. The experimental power spectra are averaged over all runs in each measurement plane. A low-pass filter has been applied to remove high-frequency noise not associated with the slow motion of interest. We obtain a good fit in both cases for $\lambda = 30\, c U_\infty^{-1}$ which is consistent with the above assumption (see Table 1). The plateau value of the response power spectrum is obtained in the limit as $\omega \to 0$, that is $G(\omega; t) \xrightarrow{\omega \to 0} \frac{A(t)}{\pi\lambda} \sim 4 \times 10^{-3} \frac{\ell^2 c}{U_\infty}$ in the last measurement plane (see Fig. 8) [32]. Fits to the other power spectra follow from setting $A(t)$ to the local variance level in the respective measurement planes. Eventually, we note that the sharp cusp in the autocorrelation as $\nu \to 0^+$ is indicative of a very short relaxation time scale of the fast dynamics t_f [53].

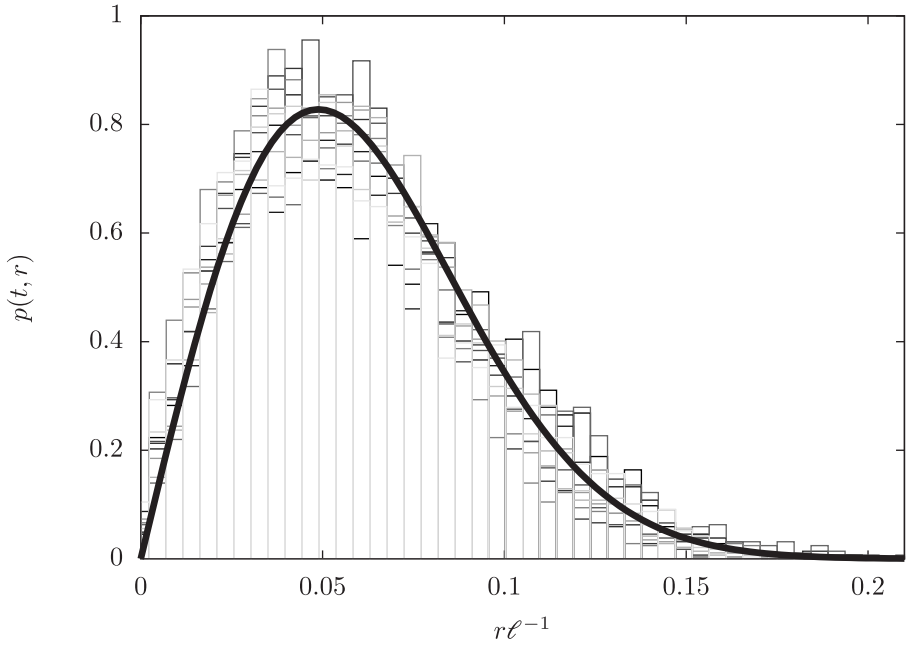

Fig. 7. Frequency distribution of the radial vortex-centre position in the last measurement plane. Histograms of individual runs (different grey shadings) and the fit of the mean over the runs to a Rayleigh probability density (thick line).

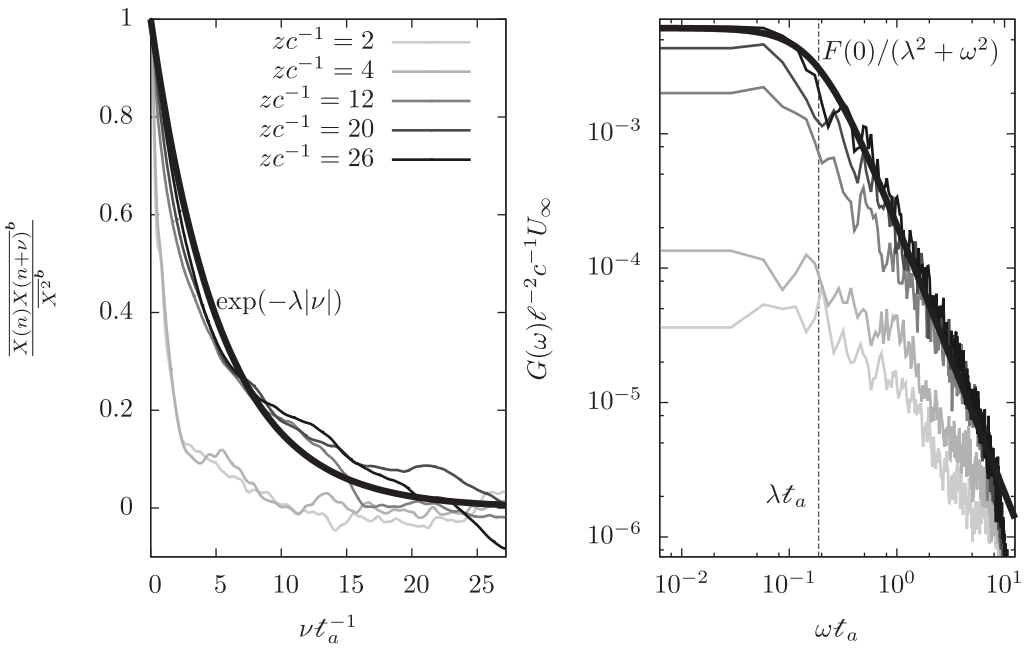

Fig. 8. Autocorrelation and power spectrum of $X(n, t = \text{const})$. Autocorrelation in the five measurement planes over time lags ν of the measurement time, compared with $e^{-|\lambda|\nu}$ for $\lambda = 30\,cU_\infty^{-1}$ (thick line). Comparison of the power spectra with $F(0)/(\lambda^2+\omega^2)$ (thick line). The dashed line at $\lambda t_a = t_s^{-1} t_a$ roughly marks the extension of the plateau.

6. Corollaries and conclusion

6.1. Features and consequences of the meandering model

Framing vortex meandering in the theory of Gauss–Markov processes, we can immediately deduce a couple of crucial aspects to characterise the dynamics. It is further possible to infer some corollaries that are necessarily implied by the theory. We shall give a brief account of some of these points in the following.

Despite turbulence, as governed by the Navier–Stokes equation, being inherently non-linear, linear (stochastic) approaches are capable of identifying key structures and mechanisms [61]. The pertinence and reliability of these results is naturally open to debate and has been questioned [5]. We have shown that under the assumption of scale separation the dynamics of one isolated coherent vortex structure embedded into incoherent turbulence is governed by a *linear* dynamics. The resulting theory of Gauss–Markov processes provides us with unambiguous characteristics of the dynamics, the validity of which we have confirmed by comparison with an experimental database and the literature. Conjectures of the linearity of coherent-structure dynamics thus far were based on the qualitative similarity of experimental and theoretical vortex response structures (cf. Fig. 2) [18,22]. This is a necessary but not sufficient criterion and the suggested models at best explained some of the key experimental features, while being in contradiction with others (e.g. growth rates, spectral signature). To the best of our knowledge, we are the first to provide convincing arguments for the linearity of vortex dynamics in real flow problems. The elements form one consistent theory that explains all key aspects of experimental vortex meandering and provide clear criteria for the limitations of the model. In particular, on the time scales of interest, Brownian motion is driven by the particular rather than the homogeneous solution, meaning that vortex dynamics constitutes a continuous forcing not an initial-value problem [40].

The here developed theory implies that no meandering is expected for ideally vanishing free-stream turbulence and the remaining dynamics would be perfectly deterministic. In the Brownian-motion analogy, this would correspond to the ceasing motion of a particle suspended in a liquid at the absolute zero temperature. The fact that the stochastic meandering is typically weak is a consequence of the conventionally low turbulence intensity ($\sim$ low-temperature dynamics) which allows deterministic dynamics to dominate the overall behaviour. Nevertheless, "[Brownian motion] excludes …the existence of "hidden periodicities" [or] "signals"" [39], or as put by [38]—"stochastic processes are neither finite nor periodic". That is, if one accepts the stochastic Brownian-motion model of coherent-vortex dynamics, the expectation to identify *the* meandering frequency must be refuted.

It is a fundamental characteristic of the statistics of turbulence that, in general, none of the stochastic moments vanishes and a complete description of the dynamics would require knowledge of the whole infinite system—this is known as the closure problem [33]. In particular, second central moments (i.e. correlations) are insufficient to determine the whole probability distribution. However, this is the case for Gaussian distributions which turn out to occur very often in practice as a consequence of the central limit theorem [32]. We have shown that this is indeed the case for the large-scale dynamics of strong isolated line vortices for which the closure problem ceases. In other words, the presented model contains the entire information of the dynamics.

6.2. Conclusion

Meandering is the paradigm of the unsteady dynamics of isolated large-scale line vortices embedded into an environment of weak small-scale turbulence. Despite its intrinsic interest as a model of a coherent structure, we find natural realisations of this flow situation with primary importance in engineering and geophysics, such as trailing or inlet vortices and tornadoes. Most experiments explore trailing vortices, so that we implicitly rely on this setting in the present study, however, expect that the results are readily generalised to comparable configurations. As such, we dispose of a large set of experimental and numerical studies, providing us with the unequivocal evidence that vortex meandering is associated with four universal main characteristics. Namely, (*i*) the vortex-centre position obeys a Gaussian probability distribution that (*ii*) monotonously broadens downstream of the vortex generator. This increase in standard deviation of the vortex-centre position is parallelled by (*iii*) an amplification of the fluctuation kinetic energy and enstrophy in the vortex core, whereas the leading-order contribution has a dipolar spatial pattern in the vorticity. Eventually, (*iv*) experimental vortex dynamics is associated with a broadband spectral signature spanning all resolved scales, whereas the variance level increases towards the low frequencies.

We present the first closed theory that explains all experimental key features in one model. Conceptually, this theory is based on the recognition that vortex meandering constitutes an integral property of a distinct large-scale object, which suggests a (Lagrangian) particle-like approach, although in an abstract sense.

Starting from the definition of the vortex centre, we first show a direct correspondence between the leading KL-mode pair of the vorticity covariance function and the (material) meandering motion observed in experiments. This association has been conjectured before, but has never been derived as far as we know. It implies that the visible meandering of the physical vortex in experiments is a manifestation of the same meandering motion in the phase space of the dynamics and that the meandering motion is truly low (viz. two) dimensional (to leading order).

On account of a scale-separation argument, we then show that the universally observed Gaussian statistics of the vortex position are a consequence of the central limit theorem. To this end, we formulate vortex meandering as a random-walk problem. It is important to realise that the thus resulting Gaussian probability distribution is a purely mathematical

consequence of summing up a very large number of subsequent (independent and identically-distributed) random steps, which is completely independent of the local probability of the vortex to make a 'step' in a certain direction.

Restriction to the leading two KL modes and scale separation allow us to write the dynamical system governing the meandering motion in the form of an abstract Langevin equation. Considering the short-time limit, this equation is solved by a Wiener process, while we get an Ornstein–Uhlenbeck process if we do not impose time restrictions. This latter includes a linear friction, or feedback term that assures convergence to an asymptotic equilibrium state in the infinite-time limit. In the light of previous explanation approaches, we conclude that the dynamics is neither completely driven by the free-stream turbulence nor due to an intrinsic vortex instability but rather a competition between external driving and internal resistance.

As of the power spectra, we show that, in equilibrium, the low-frequency range must fall off as the second power of frequency, shifted by the second power of the reciprocal vortex response time scale. This is the spectral signature of a real, symmetric autocorrelation function with exponential decay.

Comparison of our model predictions with an experimental database gathered at the ONERA leads to very good overall agreement. The experiment is consistent with all previous findings reported in the literature and the data available in these publications collapse with the derived laws. We conclude that the presented theory indeed explains experimental vortex meandering.

CRediT authorship contribution statement

Tobias Bölle: Conceptualization, Methodology, Formal analysis, Investigation, Writing.

Declaration of competing interest

The authors declare that they have no known competing financial interests or personal relationships that could have appeared to influence the work reported in this paper.

Data availability

The authors do not have permission to share data.

Appendix. Parameters of Fig. 1

The normalisation of the meandering amplitude in Fig. 1 is based on the parameters listed in Table A.2, which have been taken from the original publications. All values agree with those used in Section 5 in terms of their order of magnitude and trends upon modification of the experimental configuration.

Table A.2
Experimental parameters for meandering-amplitude scaling of Fig. 1.

	Symbol	ιU_∞^{-1}	Γ/cU_∞	Angle of incidence
[19]	□	10^{-2}	12×10^{-2}	7.5°
	□	10^{-3}	8×10^{-2}	5°
	□	10^{-3}	6×10^{-2}	3.75°
	□	10^{-3}	4×10^{-2}	2.5°
[26]	×	5×10^{-3}	10×10^{-2}	9°
[31]	○	2×10^{-3}	18×10^{-2}	5°
	○	15×10^{-3}	12×10^{-2}	5°
	○	25×10^{-3}	8×10^{-2}	5°
[67]	△	7.5×10^{-3}	10×10^{-2}	8°
[24]	▽	5×10^{-3}	25×10^{-2}	–

References

[1] A. Einstein, Über die von der molekularkinetischen Theorie der Wärme geforderte Bewegung von in ruhenden Flüssigkeiten suspendierten Teilchen, Ann. Phys. 4 (1905).
[2] M. Von Smoluchowski, Zur kinetischen theorie der brownschen molekularbewegung und der suspensionen, Ann. Phys. 326 (14) (1906) 756–780.
[3] J. Perrin, Mouvement brownien et réalité moléculaire, Ann. Chimie Phys. (1909) 5–114.
[4] P. Holmes, J.L. Lumley, G. Berkooz, Turbulence, Coherent Structures, Dynamical Systems and Symmetry, Cambridge University Press, 1996.
[5] J. Jiménez, Coherent structures in wall-bounded turbulence, J. Fluid Mech. 842 (2018).
[6] A.F. Hussain, Coherent structures and turbulence, J. Fluid Mech. 173 (1986) 303–356.
[7] J. Jimenez, A.A. Wray, On the characteristics of vortex filaments in isotropic turbulence, J. Fluid Mech. 373 (1998) 255–285.
[8] T. Miyazaki, J.C. Hunt, Linear and nonlinear interactions between a columnar vortex and external turbulence, J. Fluid Mech. 402 (2000) 349–378.
[9] N. Takahashi, H. Ishii, T. Miyazaki, The influence of turbulence on a columnar vortex, Phys. Fluids 17 (3) (2005) 035105.
[10] F. Hussain, D.S. Pradeep, E. Stout, Nonlinear transient growth in a vortex column, J. Fluid Mech. 682 (2011) 304–331.
[11] J. Marshall, M. Beninati, External turbulence interaction with a columnar vortex, J. Fluid Mech. 540 (2005) 221.
[12] S. Jammy, N. Hills, D.M. Birch, Boundary conditions and vortex wandering, J. Fluid Mech. 747 (2014) 350–368.

[13] L. Jacquin, D. Fabre, P. Geffroy, E. Coustols, The properties of a transport aircraft wake in the extended fear field: An experimental study, in: 39th Aerospace Sciences Meeting and Exhibit, 2001, p. 1038.
[14] V. Corsiglia, R. Schwind, N. Chigier, Rapid scanning, three-dimensional hot-wire anemometersurveys of wing-tip vortices, J. Aircr. 10 (12) (1973) 752–757.
[15] G. Baker, S. Barker, K. Bofah, P. Saffman, Laser anemometer measurements of trailing vortices in water, J. Fluid Mech. 65 (2) (1974) 325–336.
[16] S.C. Bailey, S. Pentelow, H.C. Ghimire, B. Estejab, M.A. Green, S. Tavoularis, Experimental investigation of the scaling of vortex wandering in turbulent surroundings, J. Fluid Mech. 843 (2018) 722–747.
[17] M. Dghim, K. Ben Miloud, M. Ferchichi, H. Fellouah, Meandering of a wing-tip vortex in a grid-generated turbulent flow, Phys. Fluids 33 (11) (2021) 115131.
[18] S. Qiu, Z. Cheng, H. Xu, Y. Xiang, H. Liu, On the characteristics and mechanism of perturbation modes with asymptotic growth in trailing vortices, J. Fluid Mech. 918 (2021).
[19] W.J. Devenport, M.C. Rife, S.I. Liapis, G.J. Follin, The structure and development of a wing-tip vortex, J. Fluid Mech. 312 (1996) 67–106.
[20] A. Antkowiak, P. Brancher, Transient energy growth for the Lamb–Oseen vortex, Phys. Fluids 16 (1) (2004) L1–L4.
[21] J. Fontane, P. Brancher, D. Fabre, Stochastic forcing of the Lamb–Oseen vortex, J. Fluid Mech. 613 (2008) 233–254.
[22] A.M. Edstrand, T.B. Davis, P.J. Schmid, K. Taira, L.N. Cattafesta, On the mechanism of trailing vortex wandering, J. Fluid Mech. 801 (2016).
[23] M. Dghim, M. Ferchichi, H. Fellouah, On the effect of active flow control on the meandering of a wing-tip vortex, J. Fluid Mech. 896 (2020).
[24] J. Van Jaarsveld, A. Holten, A. Elsenaar, R. Trieling, G. Van Heijst, An experimental study of the effect of external turbulence on the decay of a single vortex and a vortex pair, J. Fluid Mech. 670 (2011) 214–239.
[25] G.I. Taylor, Diffusion by continuous movements, Proc. Lond. Math. Soc. 2 (1) (1922) 196–212.
[26] L. Jacquin, P. Molton, P. Loiret, E. Coustols, An experiment on jet-wake vortex interaction, in: 37th AIAA Fluid Dynamics Conference and Exhibit, 2007, p. 4363.
[27] C. Roy, T. Leweke, FAR-Wake. Fundamental Research on Aircraft Wake Phenomena: Experiments on vortex meandering, Technical Report, CNRS-IRPHE, 2008, pp. 1–31.
[28] C. Del Pino, J. Lopez-Alonso, L. Parras, R. Fernandez-Feria, Dynamics of the wing-tip vortex in the near field of a NACA 0012 aerofoil, Aeronaut. J. 115 (1166) (2011) 229–239.
[29] M. Karami, H. Hangan, L. Carassale, H. Peerhossaini, Coherent structures in Tornado-like vortices, Phys. Fluids 31 (8) (2019) 085118.
[30] M. Beninati, J. Marshall, An experimental study of the effect of free-stream turbulence on a trailing vortex, Exp. Fluids 38 (2) (2005) 244–257.
[31] S. Bailey, S. Tavoularis, Measurements of the velocity field of a wing-tip vortex, wandering in grid turbulence, J. Fluid Mech. 601 (2008) 281–315.
[32] A.M. Yaglom, An Introduction to the Theory of Stationary Random Functions, Vol. 10, Prentice Hall, Englewood Cliffs, 1962.
[33] J.C. Rotta, Turbulente Strömungen: Eine Einführung in Die Theorie Und Ihre Anwendung, Vol. 15, B.G. Teubner, Stuttgart, 1972.
[34] T. Bölle, V. Brion, M. Couliou, P. Molton, Experiment on jet–vortex interaction for variable mutual spacing, Phys. Fluids 35 (2023) 015117, http://dx.doi.org/10.1063/5.0127634.
[35] D. Fabre, D. Sipp, L. Jacquin, Kelvin waves and the singular modes of the Lamb–Oseen vortex, J. Fluid Mech. 551 (2006) 235–274.
[36] T. Bölle, V. Brion, J.-C. Robinet, D. Sipp, L. Jacquin, On the linear receptivity of trailing vortices, J. Fluid Mech. 908 (2021).
[37] K. Hasselmann, Stochastic climate models part I. Theory, Tellus 28 (6) (1976) 473–485.
[38] H. Von Storch, F.W. Zwiers, Statistical Analysis in Climate Research, Cambridge University Press, Cambridge, 2003.
[39] M.C. Wang, G.E. Uhlenbeck, On the theory of the Brownian motion II, Rev. Modern Phys. 17 (2–3) (1945) 323.
[40] S. Chandrasekhar, Stochastic problems in physics and astronomy, Rev. Modern Phys. 15 (1) (1943) 1–89.
[41] E. Nelson, Derivation of the Schrödinger equation from Newtonian mechanics, Phys. Rev. 150 (4) (1966) 1079.
[42] H. Haken, Synergetics: An Introduction, second ed., Springer-Verlag, 1978.
[43] A. Libchaber, From biology to physics and back: The problem of Brownian movement, Ann. Rev. Condensed Matter Phys. 10 (2019) 275–293.
[44] H. Grabert, Projection Operator Techniques in Nonequilibrium Statistical Mechanics, Vol. 95, Springer-Verlag, Berlin, 1982.
[45] T. Bölle, Treatise on the Meandering of Vortices (Ph.D. thesis), Institut Polytechnique de Paris, 2021.
[46] G.K. Batchelor, The Theory of Homogeneous Turbulence, Cambridge University Press, 1953.
[47] J.L. Lumley, Stochastic Tools in Turbulence, Academic Press, Inc., New York, NY, 1970.
[48] H. Tennekes, J.L. Lumley, A First Course in Turbulence, MIT Press, Cambridge, MA, 1972.
[49] J. Lumley, K. Takeuchi, Application of central-limit theorems to turbulence and higher-order spectra, J. Fluid Mech. 74 (3) (1976) 433–468.
[50] A. Betz, Verhalten von Wirbelsystemen, Zeitschrift Für Angew. Math. Mech. 12 (3) (1932) 164–174.
[51] F. Riesz, B. Sz-Nagy, Functional analysis, Vol. 3, no. 6, Dover Publications, Inc., New York, 1955, First Published in.
[52] M. Loeve, Probability Theory II, fourth ed., Springer-Verlag, New York, 1978.
[53] M. Lax, Fluctuations from the nonequilibrium steady state, Rev. Modern Phys. 32 (1) (1960) 25.
[54] A.J. Majda, I. Timofeyev, E. Vanden Eijnden, A mathematical framework for stochastic climate models, Comm. Pure Appl. Math. 54 (8) (2001) 891–974.
[55] H. Mori, Transport, collective motion, and Brownian motion, Progr. Theoret. Phys. 33 (3) (1965) 423–455.
[56] R. Kubo, M. Toda, N. Hashitsume, Statistical Physics II: Nonequilibrium Statistical Mechanics, Vol. 31, Springer-Verlag, Heidelberg, 1998.
[57] R. Zwanzig, Nonequilibrium Statistical Mechanics, Oxford University Press, New York, 2001.
[58] N.G. Van Kampen, Stochastic differential equations, Phys. Rep. 24 (3) (1976) 171–228.
[59] G.E. Uhlenbeck, L.S. Ornstein, On the theory of the Brownian motion, Phys. Rev. 36 (5) (1930) 823.
[60] S.R. De Groot, P. Mazur, Non-Equilibrium Thermodynamics, Dover Publications, Inc., New York, 1984.
[61] B. McKeon, The engine behind (wall) turbulence: Perspectives on scale interactions, J. Fluid Mech. 817 (2017).
[62] J.L. Doob, Stochastic Processes, Vol. 10, New York Wiley, 1953.
[63] P. Lax, Linear Algebra and Its Applications, second ed., Wiley-Interscience, 2007.
[64] B.F. Farrell, P.J. Ioannou, Stochastic forcing of the linearized Navier–Stokes equations, Phys. Fluids A: Fluid Dyn. 5 (11) (1993) 2600–2609.
[65] B.C. Hall, Quantum Theory for Mathematicians, Vol. 267, Springer, 2013.
[66] H. Cramér, On the theory of stationary random processes, Ann. of Math. (1940) 215–230.
[67] G.V. Iungo, P. Skinner, G. Buresti, Correction of wandering smoothing effects on static measurements of a wing-tip vortex, Exp. Fluids 46 (3) (2009) 435–452.